The Corrosion of Zirconium Alloy Fuel Cladding under Deep Geological Repository Conditions

NWMO-TR-2023-04 August 2023

D. Zagidulin and D.W. Shoesmith

The University of Western Ontario

nwmo
NUCLEAR WASTE MANAGEMENT ORGANIZATION
SOCIÉTÉ DE GESTION DES DÉCHETS NUCLÉAIRES

Nuclear Waste Management Organization
22 St. Clair Avenue East, 6th Floor
Toronto, Ontario
M4T 2S3
Canada

Tel: 416-934-9814
Web: www.nwmo.ca

The Corrosion of Zirconium Alloy Fuel Cladding under Deep Geological Repository Conditions

NWMO-TR-2023-04

August 2023

D. Zagidulin and D.W. Shoesmith
The University of Western Ontario

Document History

Title:	The Corrosion of Zirconium Alloy Fuel Cladding under Deep Geological Repository Conditions		
Report Number:	NWMO-TR-2023-04		
Revision:	R000	Date:1	Month Year 8-2023
The University of Western Ontario			
Authored by:	D. Zagidulin and D.W. Shoesmith		
Nuclear Waste Management Organization			
Reviewed by:	Jose Freire-Canosa, Mehran Behazin, Tammy Yang, Mark Gobien		
Accepted by:	Paul Gierszewski		

Revision Summary		
Revision Number	Date	Description of Changes/Improvements
R000	2023-08	Initial issue

ABSTRACT

Title: **The Corrosion of Zirconium Alloy Fuel Cladding under Deep Geological Repository Conditions**
Report No.: **NWMO-TR-2023-04, R000**
Author(s): D. Zagidulin and D.W. Shoesmith
Company: The University of Western Ontario
Date: August 2023

Zirconium alloys are widely used in nuclear reactors as fuel cladding and are, therefore, a component of the waste materials that will be emplaced in a deep geologic repository. In this review, the corrosion/degradation behaviour of fuel cladding in wet and dry storage, and repository disposal conditions was reviewed. Since most of the known degradation mechanisms are inactive, no significant degradation will occur under wet or dry storage conditions.

For delayed hydride cracking (DHC), a combination of experimental and modelling investigations show that this degradation process should not be an issue during storage, despite the significant changes in temperature and the presence of hydrides in the cladding. Although hydrides will exist within the cladding, the stress intensity factor will be well below the critical value required for crack propagation.

Since zirconium and titanium are highly corrosion resistant light metals which passivate by the formation of extremely insoluble M^{IV} oxides, they exhibit many similarities, as well as instructive differences, in their corrosion/degradation behaviour, and because the data base for the corrosion of titanium alloys under general industrial and repository conditions is extensive, the electrochemical and corrosion behaviour of the two materials has been compared and evaluated. While electrochemical studies suggest Zircaloy cladding could be susceptible to localized corrosion in the form of pitting, redox conditions inside a failed waste container, established by the gamma radiolysis of groundwater, will be insufficiently oxidizing to support this process. This leaves general passive corrosion under anoxic conditions, which could lead to hydriding due to the absorption of hydrogen into the cladding, as the only significant degradation process. The available data shows that, even if the thick oxide on the cladding on discharge from reactor is ignored, the corrosion rate will be very low and conservatively within the range 1 to 5 nm/a. While the possibility that the final failure process will be due to hydriding cannot be ruled out, times to failure should be in the region of 10^5 years or longer.

TABLE OF CONTENTS

Page

LIST OF TABLES

Page

LIST OF FIGURES

Page

1. INTRODUCTION.

Currently ~3.2 million used fuel bundles have been discharged from CANDU reactors. Based on present plans for nuclear plant refurbishments and life extensions, the total number of used CANDU fuel bundles could be in the region of 5.5 million from current generating capabilities (Reilly 2022). On discharge from reactor fuel bundles will spend a minimum of 10 years under H_2O in irradiated fuel bays (IFB). Subsequently, they will be transferred to dry storage containers (DSC) for an extended period of possibly 100 years before final transport to, and disposal in, a deep geological repository (DGR). A primary need is to determine whether the fuel bundles will maintain their integrity prior to encapsulation in the sealed container. A second need is to assess the performance of the cladding assuming container failure occurs since it protects the fuel from contact with water, and once in contact with groundwater, it can act as a minor source of radionuclides formed in the cladding itself during in-reactor irradiation.

2. ZIRCONIUM AND ZIRCONIUM ALLOYS

Zirconium alloys are widely used in almost all nuclear reactors as fuel cladding and in-reactor structural elements (i.e., in CANDU reactor pressure tubes). Their choice for these applications is based on a combination of a low neutron cross section and a high corrosion resistance. Alloys presently used as fuel cladding materials include Zircaloy-2 (Zr-2), Zircaloy-4 (Zr-4) and more advanced alloys such as M5™ and Zirlo™. The compositions are given in Table 1. CANDU fuel cladding is primarily Zr-4, except for some early bundles. Current BWR fuel assemblies are primarily Zr-2 with stainless steel and Inconel components.

Table 1: Main components (in weight %) of Zr alloys used in cladding materials of fuel rods [Gras 2014].

Alloy	Zircaloy-2	Zircaloy-4	M5™	Zirlo™
Zr	Bal.	Bal.	Bal.	Bal.
Sn	1.2 – 1.7	1.2 – 1.7 *	impurity	0.9 – 1.1
Fe	0.07 – 0.20	0.18 – 0.24	0.030	0.08 – 0.12
Cr	0.05 – 0.15	0.07 – 0.13	impurity	impurity
Ni	0.03 – 0.08	impurity	impurity	impurity
O	0.08 – 0.15	0.09 – 0.16	0.140	0.100 – 0.140
C	0.008 – 0.027	0.008 – 0.027	impurity	-
Nb	impurity	impurity	1.00 ± 0.02	0.80 – 1.20
Si	0.005 – 0.012	0.005 – 0.012	impurity	-
S	impurity	impurity	0.002	-

* The maximum tin threshold for the Zircaloy-4 standard was 1.70 %. The content of low tin Zircaloy-4 now used is 1.35 ± 0.15 %.

Zr-4 is effectively Zr-2 with a reduced Ni content since evidence exists to show Ni enhances H absorption (Hillner 1964) into the alloy. The advanced alloys avoid Ni and contain small amounts of Nb to further improve the in-reactor corrosion resistance. The decrease in Ni also limits the formation of activation products, while the universal presence of Sn improves mechanical properties. Limiting the N content reduces the production of ^{14}C by neutron

activation ($^{14}N + n \rightarrow {}^{14}C + p$). The impurities Fe and Cr are insoluble in the α-Zr matrix and separate to form secondary phase precipitates (SPP) ($Zr(Fe,Cr)_2$ and $Zr_2(Fe,Ni)$) with the exact composition depending on the heat treatment of the alloy (Yilmazbayhan et al. 2006; Rodriguez et al. 2002; Degueldre et al. 2008).

During in-reactor service, CANDU fuel cladding operates at an average sheath temperature of 340 °C for about 1–2 years and receives a mainly thermal neutron fluence of around 10^{25} neutrons/m^2. While the fluence received by BWR fuel (IAEA 2005) is similar, it is for fast neutrons which would lead to more damage to the Zircaloy. The main materials processes that occur during this period are oxidation and corrosion leading to the growth of oxides on both the inner and outer surfaces, H absorption leading, at a sufficiently high concentration, to the formation of hydrides, and irradiation induced changes in alloy microstructure and mechanical properties.

Under these fluences, a number of gradual changes to the mechanical properties of the cladding occur. The formation of dislocation loops, point defect clusters involving either interstitial or vacancy sites, can lead to lattice expansion (irradiation growth (Adamson et al. 2017), hardening and a decrease in ductility (Griffiths et al. 1987), and the redistribution of impurity elements present in SPPs (Griffiths et al. 1987; Motta et al. 1991; Lefebvre and Lemaignan 1997; Etoh and Shimida 1993; Etoh et al. 1982). Of these influences, the two likely to have the largest influence on in-reactor corrosion are the amorphization of secondary phases and the generation of radiation-induced damage in the growing oxide. The latter would increase the number of defects, specifically the number of oxygen vacancies (O_V) which are utilized in oxide growth. These influences are discussed in more detail in section 3.

Irradiation also leads to the formation of neutron activation products such as ^{3}H, ^{14}C, ^{59}Ni, ^{63}Ni, ^{36}Cl and ^{93}Zr in the cladding. Although present in low concentrations, these radionuclides may be released from the Zr alloy under permanent waste disposal conditions and needs, therefore, to be considered as part of the long-term safety assessment of a DGR. A listing of cladding activation products and their concentrations in the cladding is given elsewhere (Heckman and Edward 2020). Due to the relatively low average temperature during irradiation (<340 °C), no significant diffusive transport occurs within the Zr alloy and these activation products, with the exception of ^{14}C and ^{3}H, will be uniformly distributed throughout the cladding. Some radionuclides will be present in surface deposits on the fuel cladding, from transport with the coolant. Such a distribution means these radionuclides will be released at a rate dictated by the cladding corrosion rate. The major exception is ^{14}C which has been shown to be partially enriched in the oxide on the cladding. An extensive research discussion (Gras 2014) and summary overview (Necib et al. 2018) have been published. These studies show that, while uncertainties persist, the common assumption that 20% of ^{14}C will be quickly released as part of the instant release fraction of radionuclides (those assumed to be released immediately on contact with groundwater) is overly pessimistic. However, conclusive data showing it will be released at a rate dictated by the corrosion of the cladding is unavailable. Based on screening analyses (Heckman and Edwards 2020) ^{3}T (which decays to He by β emission with a half-life of 12.3 years) is not a significant radionuclide under disposal conditions.

3. OXIDE GROWTH IN-REACTOR

The formation of a strongly adherent, insoluble oxide layer is the key feature providing the durability of zirconium alloys. The in-reactor growth of ZrO_2 on cladding has been well characterized (Garzarolli et al. 1979; Cox 1985; IAEA 1998; Tanabe et al. 2013) and reviewed (IAEA 1998; Allen et al. 2012; Motta et al. 2015). The initial thin oxide grows via the inward diffusion of O by either/both vacancy and grain boundary transport (Cox and Roy 1966; Cox and Pemsler 1968; Dollins and Jursich 1983; Zumpicchiatt et al. 2015; Tupin et al. 2003) as demonstrated by gold marker (Porte et al. 1960) and ion implantation studies (Chevalier et al. 2003; Dali et al. 2012).

Electrochemical studies show that oxide growth is driven by a high electric field across the oxide and that the electronic resistivity of the film (i.e., the resistance to the electron transport required to support H_2O reduction at the oxide/solution interface) has a significant limiting influence on oxide growth (Cox 1969). However, the Pilling-Bedworth ratio (P-B ~1.56) (Noël et al. 2000; Motta et al. 2015) induces compressive stresses at the metal/oxide interface (Wei et al. 2013; Platt et al. 2015; Godlewski et al. 2000). As stresses increase, a cracked network develops leading to film breakdown and a loss of protectiveness of what is termed the pre-transition oxide layer. Additional processes causing this transition have also been suggested (Allen et al. 2012). The kinetics of the pre-transition oxide layer growth, as measured by weight gain, follow an approximately cubic rate law (Kass 1969). Under in-reactor conditions the initial stage of growth after breakdown and the subsequent acceleration of growth is termed the post-transition stage. In the post-transition stage, growth leads to a series of parabolic growth steps, as the alloy repetitively attempts but fails to repair itself. These steps eventually merge into a linear growth process as shown in Figure 1 indicating oxide growth eventually progresses continuously.

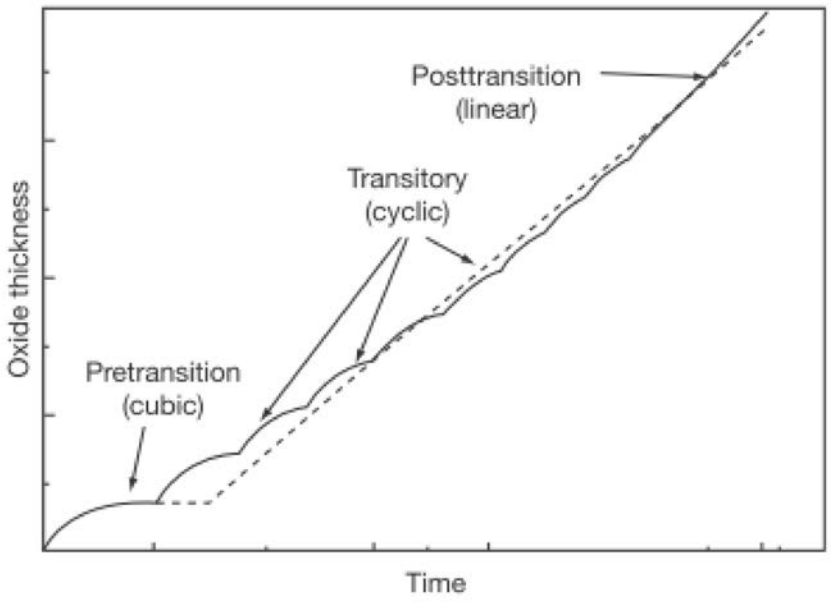

Figure 1: Schematic illustration of the oxide film growth (corrosion) process (expressed as an increase in film thickness with in-reactor exposure time) showing the pre-transition and post-transition stages.

The sequence of growth steps leads to a stratified microstructure in the oxide consisting of layers with horizontal cracks and a fine porosity which appears to be induced by tetragonal to monoclinic transformations in the film (Ni et al. 2010). Impedance and porosity measurements (IAEA 1998) suggest this fine porosity (10–100 nm) may penetrate close to, if not up to, the Zr/oxide interface and there is no unequivocable evidence to support the reformation of an oxide barrier (pre-transition) layer once the porous structure has developed and post-transition kinetics have been established. As discussed in Appendix A, once breakdown has been induced electrochemically, there is good evidence from neutron reflectometry studies on ZrO_2 films on Zr that H_2O can penetrate the oxide film with its reduction at the metal surface leading to H absorption into the metal (Noël et al. 2008). In the post-transition region, therefore, linear growth can be supported by more facile transport processes within the porous structure which allows access of H_2O to the alloy/oxide interface. These observations are consistent with results which show H absorption follows the sequence of oxide transitions at least up to the third transition (Tupin 2003; Couet et al. 2014; Harada and Wakamatsu 2008; Une et al. 2011).

Comprehensive reviews of cladding corrosion and models describing growth kinetics have been published (Cox 1976, 1990; IAEA 1998; Allen et al. 2012; Adamson et al. 2007; Motta et al. 2015). The thickness of the oxide layer (equivalent to the extent of corrosion) depends on the in-reactor burnup and the composition of the alloy (Bossis 2006), Figure 2. For Zr-4 the oxide thickness increases with burnup especially for burnups greater than approximately 40 MWd/kgU. It has been claimed that the acceleration in film growth at high burnups can be attributed to the formation of hydrides in the alloy surface since pre-charging of the alloy with H led to an increase in corrosion rate (Blat and Noel 1996; Blat et al. 2000). Since the burnup of CANDU fuel is restricted to 7.5–9.5 MWd/kg(U), the film thickness would be expected to be 3–4 µm which is close to the measured value of ~5 µm (Gras 2014; Gobien et al. 2018). Since burnups for PWR and BWR are considerably higher, oxide thicknesses are consequently higher with BWR cladding experiencing slightly more extensive corrosion due to the aggressive steam environment although the growth mechanism remains the same. For BWR fuel cladding at a burnup of 40 to 50 MWd/kgU, the film thickness would be in the range 30–50 µm with thicknesses up to 150 µm having been reported. The extent of corrosion is significantly limited by the addition of Nb to the M5^{TM} alloy.

Examination of the region close to the alloy/oxide interface showed a complicated structure. TEM studies suggest the microstructure described above extended to the interface suggesting no barrier layer was present. An oxide gradient was observed in the alloy surface indicating O diffusion into the alloy to form a suboxide. Within this suboxide, the O level exceeds the ~29% solubility limit for O in α-Zr, leading to the precipitation of small ZrO_2 crystallites. For oxides grown on Zr-2 (500^{o}C for ~144 hours), mass spectroscopy measurements (Hutchinson et al. 2007) showed that, while the film at the oxide/solution interface was stoichiometric ZrO_2, an O concentration gradient was present over a 150 nm to 400 nm region close to the Zr-2/oxide interface, indicating a composition approaching ZrO at the interface. Such a region suggests the presence of a barrier layer not detected in the TEM studies. An electrochemical impedance study on Zr (0.25 Sn, 0.11 Fe, 0.01 Cr, 0.01 Ni (wt%)) in $B(OH)_3$ containing 0.001 LiOH (at 250^{o}C) was similarly inconclusive (Ai et al. 2008). Despite assuming in the modelling of the impedance data that a barrier layer was present, the results in the latter study indicated that the corrosion resistance was dominated by the porosity of the outer layer.

In the study on Zr-4 (Yilmazbayhan et al. 2006), the oxidation front was found to bypass the secondary phase precipitates (SPP) (Zr_2(Fe,Ni) and Zr(Fe,$Cr)_2$) present in the alloy, which are known to have a higher oxidation resistance than the Zr matrix (Pecheur et al. 1992, 1994) leading to their incorporation into the oxide in the unoxidized metallic form. Many metallic SPPs

were observed in the oxide near the alloy/oxide interface, but beyond a certain distance from the interface they existed in the oxidized form. The size and distribution of SPPs in Zircaloys have been shown to influence in-reactor corrosion kinetics (IAEA 1998) and electrochemical evidence exists to demonstrate they act as preferential cathodes. Other studies have also demonstrated that their oxidation rate is lower than that of the matrix Zr, leading to a decrease in in-reactor corrosion kinetics (IAEA 1998).

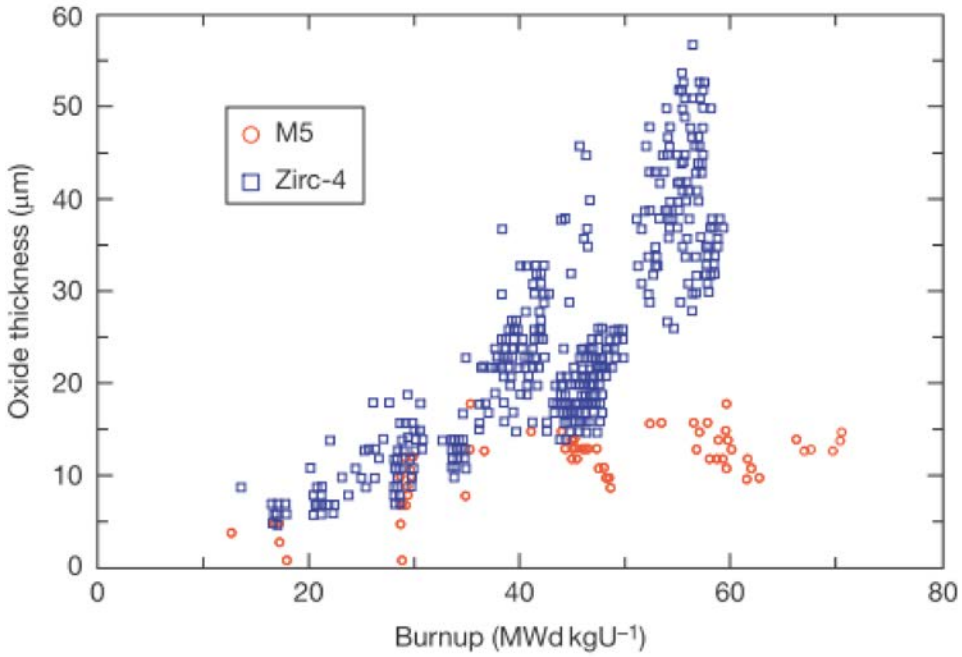

Figure 2: Oxide film thickness as a function of in-reactor burnup for Zr-4 and Alloy M5™ [Gras 2014]. The oxide thickness on Zr-2 (used in BWRs) could be slightly less than that on Zr-4 (used in PWRs) due to the lower operating temperature in BWRs [Motta et al. 2015].

The influence of SPPs on H profiles in the pre-transition oxide film has been demonstrated by SIMS (Hatano et al. 1996). By comparing the amount of H in the films on steam-oxidized Zr-2 containing either fine or coarse-grained SPPs, it was demonstrated that their retention in the unoxidized form in the oxide matrix (as was the case for coarse-grained precipitates) increased the rate of H transport in the oxide. The rate controlling process was transport through the oxide with periods of rapid transport through the unoxidized intermetallics, which, as a consequence of their 3d metal content, have a large affinity for H (e.g., $Zr(Fe,Cr)_2$ can absorb H up to a composition of $ZrFeCrH_3$ (Shaltiel et al. 1997)). Once film breakdown has occurred and the alloy is in the post-transition stage H absorption into the alloy will be facilitated by the access of H_2O to the alloy/oxide interface (as discussed in Appendix A). Corrosion of the SPPs in the oxide leads to the doping of the associated oxide with subvalent cations (Fe^{III}, Cr^{III}, Ni^{II} in the Zr^{IV} lattice). This leads to an increase in the number of O vacancies which act as holes to increase the conductivity of the ZrO_2 barrier layer (i.e., the pre-transition oxide) possibly enabling such locations to act as preferential cathodes, although this requires confirmation.

The evidence in support of a barrier layer under high temperature conditions is ambiguous and it may be that its absence is necessary to sustain the linear oxidation rate observed over the

post-transition in-reactor exposure period. However, on removal from the reactor when oxide growth is no longer driven by high in-reactor temperatures, a barrier layer would be expected to form at any exposed Zr locations. Attempts to measure any barrier layer thickness for post-transition oxides suggest, if they exist, they are extremely thin (Cox 1968).

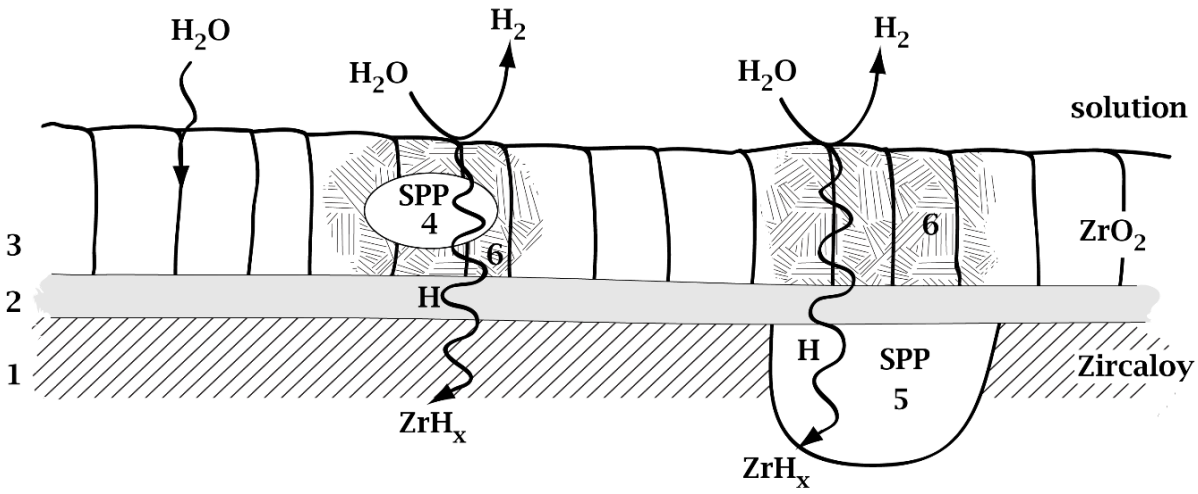

Figure 3: Schematic showing a simplified summary of the various features of oxide films formed in-reactor on Zircaloy: (1) O dissolved in the α-Zr matrix; (2) ZrO_2 barrier layer; (3) columnar, crystalline ZrO_2 oxide; (4) unoxidized secondary phase particles (SPP) isolated within the oxide film; (5) SPPs in, or in contact with the Zircaloy matrix; and (6) subvalent-doped ZrO_2 with enhanced electrical conductivity produced by oxidation of SPPs.

An attempt to summarize (in simplified form) the various properties of the oxide is shown in Figure 3. The following features can be identified:

1. A region within the α-Zr matrix containing dissolved O.

2. A thin ZrO_2 layer with a depleted O content which may/may not comprise a barrier layer at the alloy/oxide interface.

3. An outer columnar, crystalline ZrO_2 film, with a thickness dependent on burnup, containing a network of pores which allow access of H_2O to the alloy/oxide interface. It is possible, but not demonstrated that this access is blocked by the formation of a thin barrier layer.

4. SPPs isolated in the metallic form in the outer layer oxide which can incorporate significant quantities of H and facilitate its transport into the Zircaloy matrix.

5. SPPs in, or in contact with, the Zircaloy matrix which can also facilitate H transport into the alloy.

6. Areas of subvalent-doped ZrO_2 with enhanced electrical conductivity produced by oxidation of SPPs.

4. ABSORPTION OF HYDROGEN IN-REACTOR

The in-reactor corrosion of Zr cladding proceeds via reaction with H_2O to produce H_2

$$Zr + 2H_2O \rightarrow ZrO_2 + 2H_2 \quad (1)$$

with the fraction of H absorbed by the alloy specified as the H pick-up fraction (~15%) (Kammerzind et al. 1996; Couet et al. 2014a, 2014b). This H remains in solution providing its concentration does not exceed the terminal solid solubility (TTS) for H in the alloy (Kammerzind et al. 1996; Kearns 1967; Eriksen and Hardie 1964; McMinn et al. 2000; Une and Ishimoto 2003) which is in the range of 150 ppm at 350 ^oC. Beyond this limit, precipitation as δ-ZrH_x ($1.5 \leq x \leq 1.66$) oriented perpendicular to the tensile stress occurs (Gras 2014). The amount of H absorbed is dependent on the extent of in-reactor corrosion and hence related to the degree of fuel burnup (Bossis et al. 2006; Mardon 2008) as shown in Figure 4 for Zr-4 and M5™. The influence of Nb content on reducing the extent of corrosion, and hence the amount of H absorbed, is clear in Figure 4. The possible reasons for this have been discussed by Motta et al. (2015). It has been claimed that the acceleration of corrosion/H absorption at high burnup is attributable to the presence of hydrides (Ensor et al. 2017; Motta et al. 2015). For CANDU fuel burnups, which are in the range 7.5 to 9.5 MWd/kg(U) such an amplification process would not occur but would be expected for BWR fuel with burnups in the range 40 to 50 MWd/kgU

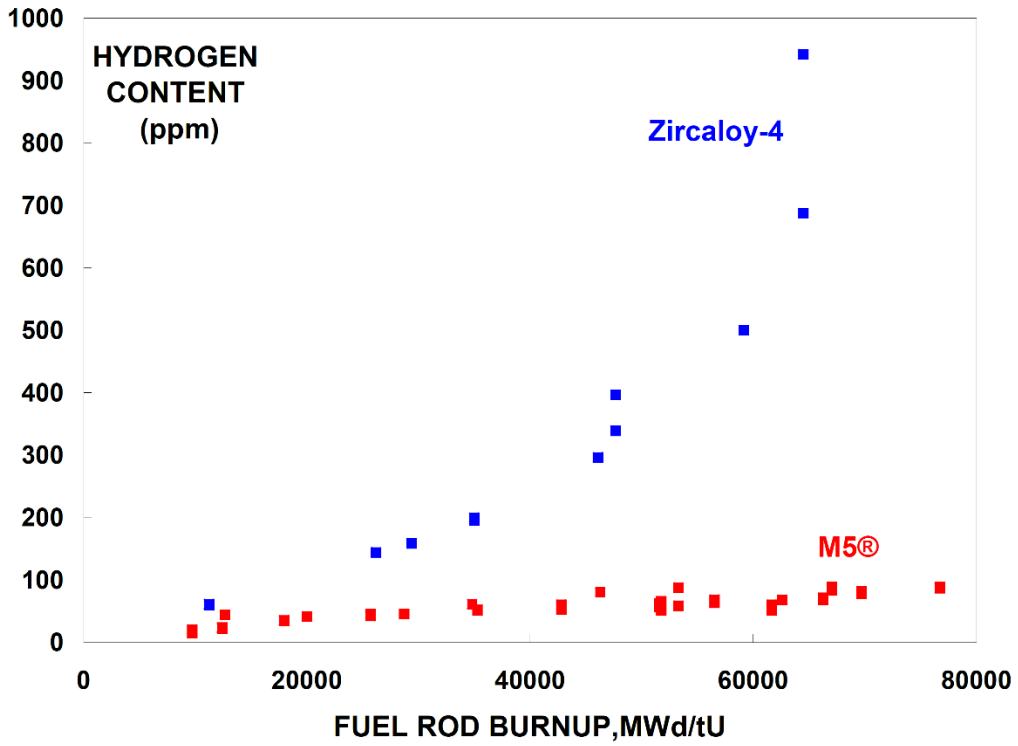

Figure 4: The amount of hydrogen absorbed by Zr-4 and the M5™ alloy as a function of in-reactor burnup [Gras 2014].

5. BEHAVIOUR UNDER WET AND DRY STORAGE CONDITIONS

Spent fuel behaviour under wet and dry storage conditions has been extensively studied internationally with the results of over 50 years of wet and 30 years of dry storage described in detail in summary reports (Bradley et al. 1981; IAEA 2006, 2015, 2019, 2021). Under wet storage conditions (i.e., while the fuel is in reactor IFBs), no observable degradation via possible uniform and local corrosion (pitting, galvanic corrosion, microbial corrosion processes) was observed. In studies summarized by Gras (2014), under no circumstances (as polished, oxidized, hydrided) was Zr-4 found to be susceptible to pitting in H_2O (pH = 5.5) containing 1 g/L of Cl^- at 80°C despite the conditions being oxidizing. A similar lack of susceptibility would be expected for Zr-2 given its compositional similarity to Zr-4 (Table 1). For the M5™ alloy a possible susceptibility to pitting was observed at 80 °C under acidic conditions but not in neutral to alkaline solutions. These observations are not surprising considering the relatively short (~10 years) storage period and the benign IFB conditions (low temperature and relatively clean H_2O).

In a study of CANDU fuel (Wasywich 1992) examined the condition of 35 fuel elements from 14 different bundles (with burnups ranging from 43 to 217 MWh/kg·U) exposed to conditions resembling those prevailing in an IFB for periods from ~13 to ~27 years. The results can be summarized as follows:

- No apparent changes in condition of the oxide on the cladding outer surfaces were observed.

- Some Zr hydride platelet alignment was observed at an end plate/end cap weld junction in an element stored for 13 years. Similar observations were made at the end cap/cladding weld junctions of 3 elements stored for 13, 17 and 26 years. While it was suspected this occurred during in-reactor irradiation it raised the possibility of delayed hydride cracking (DHC) during storage.

- There was no evidence of H-pick-up, the measured amounts not having changed measurably over the storage period.

- No apparent H-build-up or cladding degradation was detectable in metallographic cross sections.

This, and further evaluations of possible degradation mechanisms, led to the conclusion that used CANDU fuel bundles are unlikely to suffer significant mechanical degradation during the extended dry storage period, since most of the cladding degradation mechanisms which could occur are not active under storage conditions (Byrne and Freire-Canosa 1984; Lovasic and Villagran 2004; Lovasic and Gierszewski 2005; Lampman and Daniels 2005). However, uncertainties remained over hydride behaviour during wet storage and whether the stress levels, particularly at the assembly welds, would be sufficient to initiate and propagate DHC.

DHC is a process driven by H/D diffusion in a stress gradient to high stress locations at which hydride precipitation can occur if the terminal solubility of H is exceeded (Kammerzind et al. 1996; McMinn et al. 2000; Une and Ishimoto 2003; Motta and Chen 2012). The temperature increase experienced by the fuel on the transfer from the IFB to the DSC (~25 °C to 150 °C) can result in redissolution of hydrides formed under the low temperature pool storage conditions, and in an increase in internal pressure in the fuel bundle. Subsequently, cooling over the extensive dry storage period allows reprecipitation of hydrides. In Zr-4, this leads to hydride platelets perpendicular to the stress which eventually results in the initiation of a fracture.

Depending on the H/D content, this process continues in stages until either the stress is relieved, or the propagating fracture leads to failure.

For failure to occur, the two necessary conditions are that the [H] ([D] in CANDU cladding) exceeds the solubility at the prevailing temperature and the stress level must be sufficient to maintain H (D) migration till failure. Analyses show that the discharged CANDU fuel bundles contain a [D] in the range 45–88 ppm (Lampman and Gillespie 2010) which is well in excess of the solubility at dry storage temperatures (~150 ^{o}C) of 20 ppm by weight. Consequently, whether or not DHC will occur becomes a question of whether stress enhancement at susceptible locations, such as the fuel bundle assembly weld region, can exceed the critical stress intensity factor required to support DHC at this location.

A comparison of finite element CANDU fuel bundle stress models (Lampman and Popescu 2008, 2010; Popescu and Lampman 2010) and experimental measurements of the stress intensity factor required to initiate DHC (Shek and Wasiluk 2009; Shek 2010, Lampman and Popescu 2010) was performed. These calculations and measurements showed that, based on studies on both 28 and 37 element bundles, the calculated stress intensity factors of ≤3 MPa·m$^{1/2}$ were well below the critical values which were in the range 7.6 to 13.6 MPa·m$^{1/2}$. Since the calculated values are well below the critical values, DHC is not expected for CANDU fuel under dry storage conditions, with the significant margin between values sufficient to cover remaining uncertainties.

A number of studies have investigated the possibility of DHC under dry storage conditions for PWR/BWR fuel (Brady and Hanson 2020; IAEA 2015; Ahn 2019; Epri 2020; Hong et al. 2021). While most studies are on PWR cladding, BWR cladding can be considered bounded by that of PWR cladding. As for CANDU cladding, the stress levels were calculated to be significantly below the threshold stress intensity factor, with recent evaluations (IAEA 2015; EPRI 2020) showing that, over a range of realistic hoop stresses, the critical crack size required to sustain DHC was unrealistically large (i.e., greater than the cladding thickness).

6. BEHAVIOUR UNDER PERMANENT DISPOSAL CONDITIONS

The accepted concept for the permanent disposal of used nuclear fuel is burial in a deep geological repository (DGR) consisting of multiple natural and engineered barriers to isolate the nuclear waste from the environment. The proposed disposal plan in Canada involves the encapsulation of the waste in a used fuel container (UFC) surrounded by a highly-compacted bentonite buffer emplaced at a depth ≥500 m in a stable geological formation. The key engineered component is the UFC comprising a carbon steel vessel with an ~3 mm-thick Cu coating, applied via electrodeposition and cold spray deposition technologies, acting as the corrosion barrier (Keech et al. 2014; Boyle and Meguid 2015; Vo et al. 2015). While the container will provide long-term containment (Hall et al. 2021), repository performance assessments require consideration of the consequences of its failure which could lead to the exposure of the fuel bundles to groundwater.

Table 2: Reference groundwater compositions for crystalline (CR-10) and sedimentary (SR-290-PW) host rocks [Hall et al. 2021; Colás et al. 2022].

	Water Type	
	CR-10[a]	**SR-290-PW[b]**
	Nominal pH	
Acidity	7.0	5.5
Solutes	*Concentration (mg L^{-1})*	
Na^+	1,900	51,306
K^+	15	8673
Ca^{2+}	2,130	41,481
Mg^{2+}	60	7249
HCO_3^-	70	16
SO_4^{2-}	1,000	264
Cl^-	6,100	174,208
Br^-	<1	2296
Sr^{2+}	25	1101
Li^+	<1	9
F^-	2	0.3
I^-	<1	14
B		158
Si	5	4
Fe	1	5
NO_3^-	<1	<5
PO_4^{3-}	0	<0.1
TDS[c]	11,300	286,782

[a] Na-Ca-Cl, characteristic of waters from a depth of 350-800 m in crystalline rock
[b] Na-Ca-Cl, characteristic of waters from a depth of 400-700 m in limestone sedimentary rock
[c] TDS = total dissolved solids

6.1 GROUNDWATER COMPOSITION

The composition of the groundwater entering a failed container will depend on the type of host rock and the interaction between groundwater and the surrounding clay as DGR conditions evolve with time. Groundwater compositions from relevant Canadian sedimentary rocks and crystalline rocks have been measured and reference compositions for a generic site are shown in Table 2 (Hall et al. 2021: Gobien et al. 2016; NWMO 2017, 2018).

Both chemical analyses and the application of speciation codes and ion-exchange expressions have been used to determine the influence of evolving DGR conditions on the groundwater composition and on the solubility of radionuclides that could eventually be released (King et al. 2017; Colás et al. 2021, 2022). Based on these studies the groundwater entering a failed container will be anoxic with a pH in the range 5.5 to 7 (Table 2). The key groundwater species that could possibly influence corrosion/radionuclide release processes within the container are Cl^-, SO_4^{2-}, HCO_3^-, Na^+ and Ca^{2+}, pH and soluble Fe from corrosion of the steel container (Colás et al. 2021, 2022). Any O_2 introduced into the near field environment during construction of the DGR and its operation prior to sealing will have been consumed by mineral and biochemical reactions in the clay surrounding the emplaced containers and by corrosion of the Cu coating and carbon steel vessel (King et al. 2017; Hall et al 2021).

Consequently, the redox conditions within a failed container will be controlled by the radiolysis products formed by the radiation fields associated with the waste, and how they are influenced by reactions with corrodible surfaces, specifically the fuel and steel vessel and the cladding. The evolution in radioactivity is shown for reference CANDU fuel (with a burnup of 220 MWh/kgU) (Heckman and Edward 2020) in Figure 5 and the alpha, beta and gamma radiation dose rates as a function of time, Figure 6 (Ariani 2022). For the inside surfaces of the cladding, the radiation dose rates will be similar to those at the fuel surface, while only gamma radiation, at a dose rate attenuated by the cladding, will be present on the outer surfaces of the cladding. Any influence of neutron irradiation on cladding corrosion has been shown to be insignificant (Yang et al. 2019).

As noted above, the fuel will be in dry storage for a period of up to 100 years. A majority of the gamma (γ) emitting fission products in the fuel and activated impurities within the cladding will decay within this storage period beyond which the radioactive decay process will be dominated by α-particle emission predominantly from the actinide content of the fuel (Figure 6). For the cladding, two scenarios can be envisaged: intact cladding, when groundwater contacts only the outer surface of the cladding, and failed cladding when groundwater could bring it into galvanic contact with the fuel. For intact cladding, only γ-radiation is sufficiently penetrating to produce radiolysis products at the outer cladding surface. Given the extended dry storage period and a minimal containment period by the UFC in the DGR after emplacement, γ-radiation fields should have decayed to insignificant levels prior to contact of the cladding with groundwater, Figure 6.

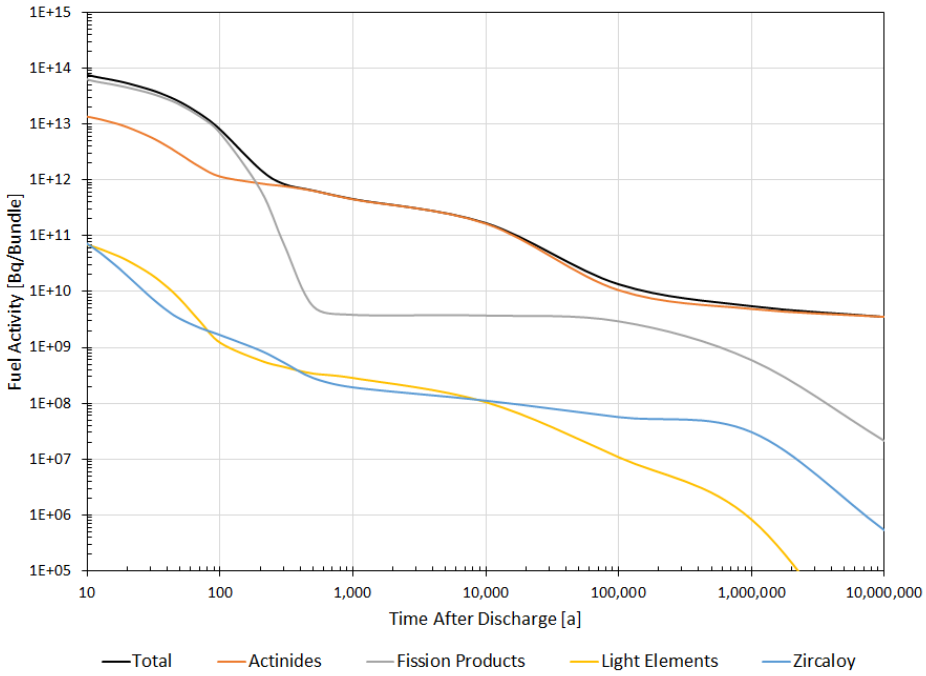

Figure 5: Radioactivity of Reference CANDU Used Fuel (220 MWh/kgU Burn-up) as a Function of Time after Discharge from Reactor [Gobien et al. 2022].

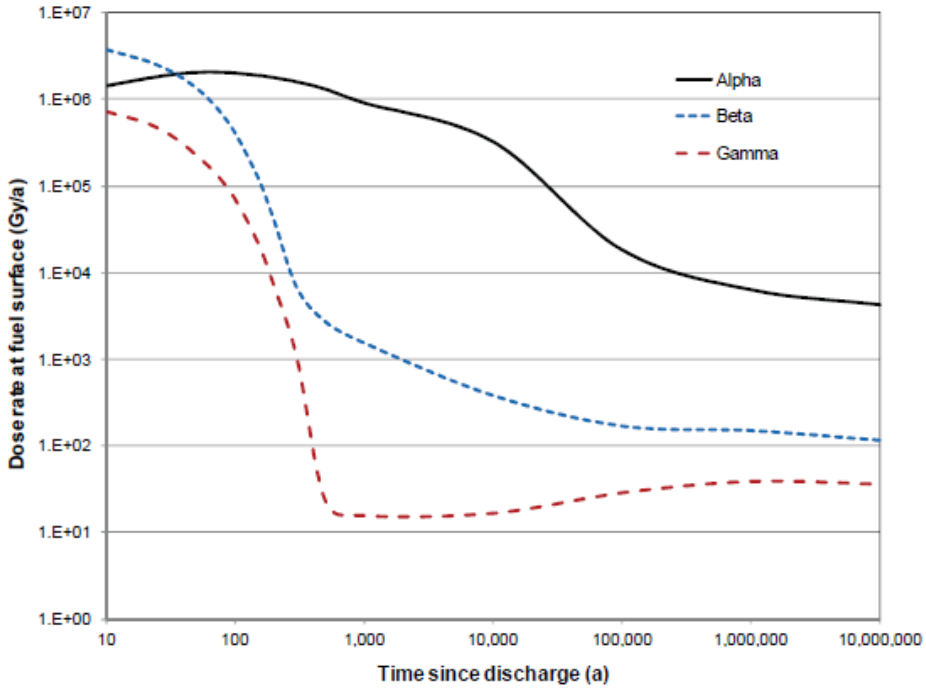

Figure 6: Alpha (α), Beta (β) and Gamma (γ) Dose Rates as a Function of Time for a Layer of Water in Contact with Fuel with a Reference Burnup of 220 MWh/kgU [Ariani 2023].

If container failure did occur during the early post emplacement stage, it is possible the cladding could be exposed to air with an uncertain humidity level containing small amounts of gases (H_2S, N_2, CO, CO_2, NO_x infiltrated from the open tunnels (King et al. 2017; Hall et al. 2021). Additionally, the radiation fields present would be significant and radiolysis of N_2/H_2O could produce HNO_3. Since the oxide covered cladding will be both chemically inert and redox insensitive, these species would be scavenged by the active container materials. Both H_2S and CO/CO_2 would react readily with both Cu and steel (Hall et al. 2021, Lee et al. 2006; Goldman et al. 2020a, 2020b; Sherar et al. 2013). In support of these conclusions there is no reported evidence to show Zr and its alloys react with any of these species (Yau 2005; Yau and Sutherlin 2005). The gamma radiation dose rate to internal surfaces has been calculated for standard CANDU fuel (Morco et al. 2017) and the extent of HNO_3 formation determined. The HNO_3 produced, as well as any NO_x introduced from the tunnels, would be consumed by reaction with the carbon steel vessel and the Cu container both of which actively corrode under these conditions (Li et al. 2013; Turnbull et al. 2018), not by the Zr cladding which would remain passive and unreactive (Gwinner et al. 2022) due to the presence of the oxide film grown in-reactor.

In the anoxic groundwater that will eventually prevail, any significant effect of radiolysis on groundwater redox conditions will be suppressed by Fe^{2+} and H_2 produced by corrosion of the steel vessel. Under anoxic conditions the steel corrosion potential will be low (≤−800 mV (vs SCE)) (Blackwood et al. 1995; Smart et al. 2002a, 2002b) restricting corrosion to the Fe^{2+} state with a solubility of iron in the 10^{-3} to 10^{-5} mol/L for the anticipated groundwater pH range, Figure 7.

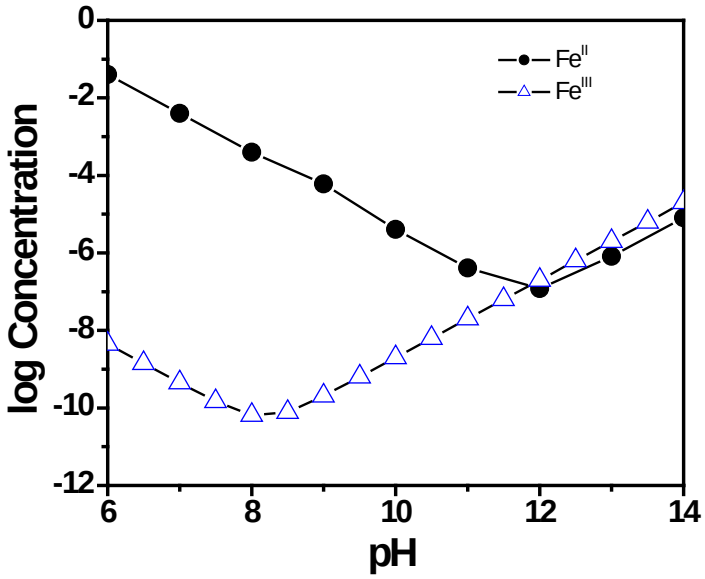

Figure 7: Solubility of Fe^{2+} and Fe^{3+} oxides as a function of pH.

$$Fe + 2H_2O \rightarrow Fe^{2+} + H_2 + 2OH^- \quad (2)$$

$$3Fe + 4H_2O \rightarrow Fe_3O_4 + 4H_2 \quad (3)$$

Hydrogen is known to suppress the production of radiolytic oxidants by γ-radiolysis (Pastina et al. 1999; Pastina and LaVerne 2001) by reactions such as

$$H_2 + OH^{\bullet} \rightarrow H_2O + H^{\bullet} \quad (4)$$

$$H^{\bullet} + H_2O_2 \rightarrow H_2O + OH^{\bullet} \quad (5)$$

$$H^{\bullet} + O_2 \rightarrow HO_2^{\bullet} \quad (6)$$

$$H^{\bullet} + HO_2^{\bullet} \rightarrow H_2O_2 \quad (7)$$

and H_2O_2 is rapidly consumed by reaction with dissolved Fe^{2+} (Barb et al. 1951; Sutton and Winterbourn 1989; Zepp et al. 1992; King and Stroes-Gascoyne 1992; Johnson and Smith 2000).

$$Fe^{2+} + H_2O_2 \rightarrow Fe^{3+} + OH^{\bullet} + OH^{-} \quad (8)$$

$$Fe^{2+} + OH^{\bullet} \rightarrow Fe^{3+} + OH^{-} \quad (9)$$

Any Fe^{3+} produced in this manner would be precipitated as Fe^{III} solids, since the solubility of Fe^{3+} is many orders of magnitude lower than that of Fe^{2+} at anticipated groundwater pHs, Figure 7.

For failed cladding, similar redox scavenging reactions would be anticipated. In this case α-radiolysis to produce molecular oxidants (H_2O_2) (Figure 6) would be most likely to influence groundwater redox conditions. However, there is a considerable accumulation of evidence to show that H_2, produced both radiolytically and more copiously by steel corrosion, can effectively eliminate the oxidizing influence of radiolytically-produced oxidants (Broczkowski et al. 2010; Badley and Shoesmith 2022). A more general discussion of radiation effects is given in section 9.

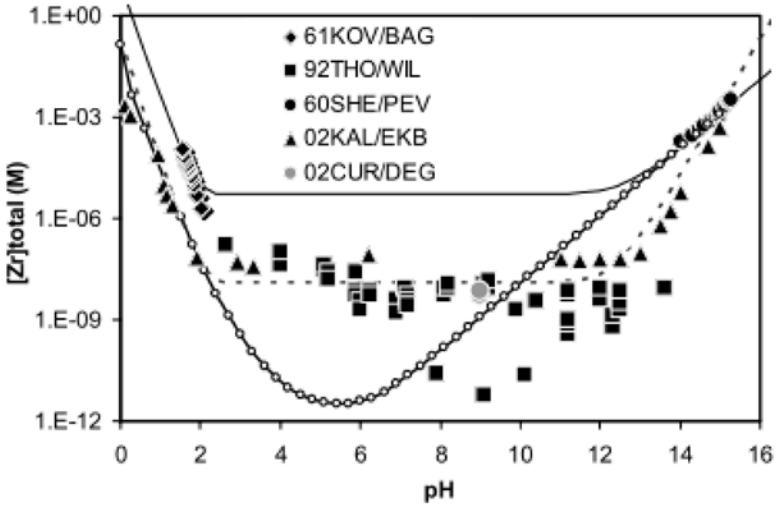

Figure 8: Solubility values for ZrO_2 in water compiled from a number of sources [Andra 2005]. The connected open circles show values calculated based on hydrolysis constants given by Baes and Mesmer [1976]. The data points are from the specific publications noted on the figure panel which are listed in Gras (2014).

7. SOLUBILITY OF ZRO_2

The solubility of ZrO_2, which would be expected to be a major influence on its chemical dissolution rate from cladding surfaces, has been reviewed in detail (Gras 2014; Curti and Degueldre 2002). The rates obtained depend on how the oxide was formed, with fresh precipitates yielding unrepresentative high values (Kobayashi et al. 2007). Crystallized oxide, which would be more representative of that present on cladding surfaces, yields values in the range of 10^{-8} to 10^{-9} mol/L over the pH range 3 to 12, Figure 8, and Bruno et al. (1997) have proposed a solubility of 10^{-9} mol/L as a conservative estimate for this pH range. However, calculations based on constants for the hydrolysis reactions for crystalline ZrO_2

$$Zr^{4+} + xH_2O \rightarrow Zr(OH)_x^{(4-x)+} + xH^+ \quad (1 \leq x \leq 4) \qquad (10)$$

tabulated by Baes and Mesmer (1976), which fit low and high pH values well, predict solubilities approaching 10^{-12} mol/L in the pH range 4 to 6 (the connected open circles in Figure 8) with values of ~10^{-10} mol/L for the upper pH limit of ~ 7.7 expected in a Canadian DGR (Table 2). The observation, noted by Gras (2014), that no ZrO_2 dissolution is detectable in in-reactor primary H_2O is consistent with such a low solubility.

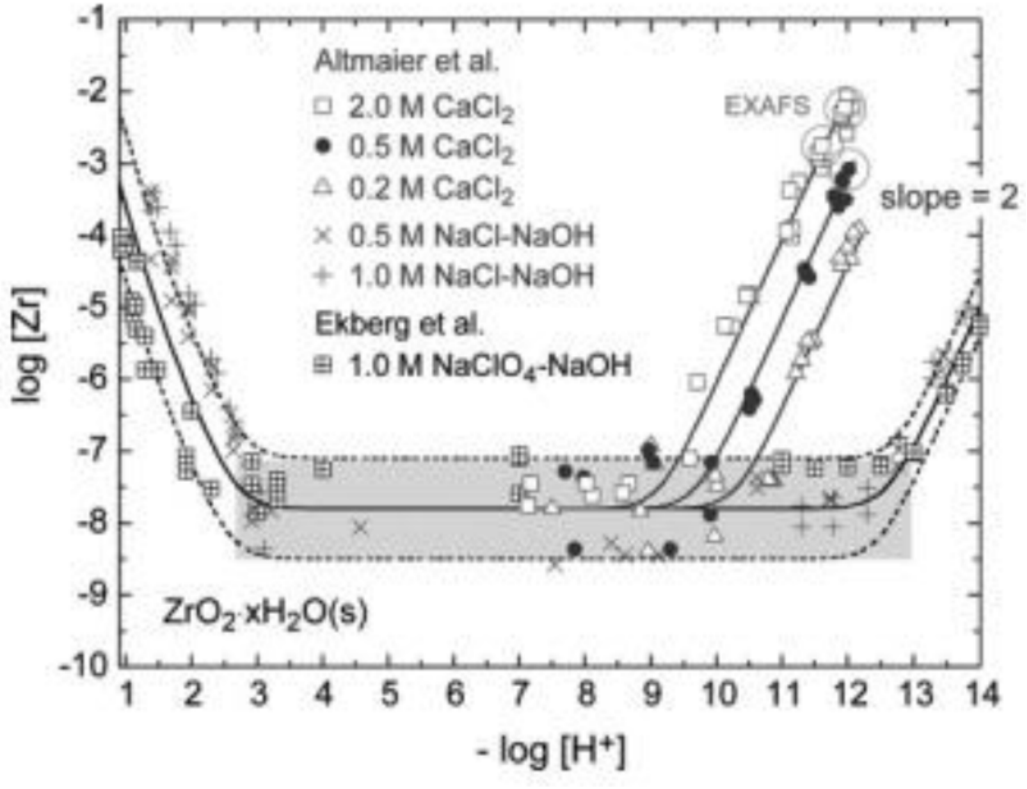

Figure 9: Solubility of $ZrO_2 \cdot xH_2O$ in $NaClO_4$, NaCl and $CaCl_2$ solutions at 20–25°C [Brendebach et al. 2007].

Within the pH range 5.5 to a maximum of 9 anticipated in a Canadian DGR, Figures 8 and 9, the pH will exert a negligible influence on ZrO_2 solubility and, hence, on its dissolution rate. Of the species present in Canadian groundwaters (Table 2) those which complex Zr^{4+} could influence the solubility of ZrO_2. On its own Cl^-, the most concentrated groundwater anion in a Canadian

DGR is unlikely to have any significant influence on the solubility, Figure 9 (Brendebach et al. 2007).

However, in the presence of Ca^{2+}, also potentially present at high concentrations in reference groundwaters (Table 2), the solubility of zirconium hydrous oxides increases markedly for pH>9 when ternary $Ca_3[Zr(OH)_6]^{4+}$ complexes can form (Brendeback et al. 2007). Since these measurements were conducted at room temperature, there is a concern that dissolution could be accelerated at high temperatures leading to more rapid dissolution at DGR temperatures (up to 90ºC). That this will not be the case has been demonstrated by Qui et al. (2009) and Kobayashi et al. (2013).

At high $[HCO_3^-]$ (>10^{-2} mol/L) the solubility increases to ~10^{-6} mol/L due to the formation of carbonate complexes such as $Zr(CO_3)_5^{6-}$ and $Zr(OH)_3CO_3^-$ (Curti and Hummel 1999; Hummel et al. 2002). Since the carbonate concentrations at the DGR conditions will be in the 1 to 2 mM range, the solubility of ZrO_2 is unlikely to be significantly influenced.

If a sufficient $[F^-]$ is present, Zr is soluble as a ZrF_6^{2-} complex. Thermodynamic calculations in the form of a potential-pH (Pourbaix) diagram show a pH≤1 is required for ZrO_2 to be soluble at a concentration of 10^{-6} mol/L in a solution containing $[F^-]$ = 0.1 mM (similar to that in the reference groundwater CR-10 (Table 2)) (Lowalekar and Raghavan 2004). For a significant solubility to be achieved the pH must be <5 which is below the minimum pH expected in Canadian repository groundwaters (Table 2).

8. CORROSION

Based on studies on the surface properties of oxide films formed on Ti and Zr and their alloys (Appendix A), the key processes which could lead to corrosion of Zr alloys are the following: (1) passive corrosion controlled by the chemical dissolution of the oxide; (2) H absorption due to H_2O reduction which could lead to embrittlement; (3) passive film breakdown leading to pitting.

Other forms of corrosion can be ruled out. As noted by Gras (2014) stress corrosion cracking (SCC) is not expected for Zr alloys under DGR conditions, and there are no published examples of microbially-induced corrosion of Ti or Zr materials. In the case of Ti there is a substantial literature to support this conclusion (Mansfeld et al. 1990, 1992, 1994; Mansfeld and Little 1991; Little et al. 1992, 1993). While there is a possibility of galvanic corrosion of Ti, leading to its H embrittlement when coupled to active materials (such as carbon steel), this is not the case for Zr alloys. As discussed in Appendix A and summarized below the oxide film on Ti can be reduced at potentials possibly achievable by coupling to carbon steel which could lead to galvanic corrosion. By contrast, the oxide film on Zr alloys is irreducible at potentials which might be achievable by inadvertent coupling to the steel containment vessel. This inability to induce conductive defects allows the cladding to maintain its insulating properties and renders it unable to support a galvanic coupling process. This conclusion is consistent with general observations for zirconium which show excellent resistance to galvanic corrosion even under conditions much more extreme than those possible in a DGR (Yau 2005; Yau and Sutherlin 2005).

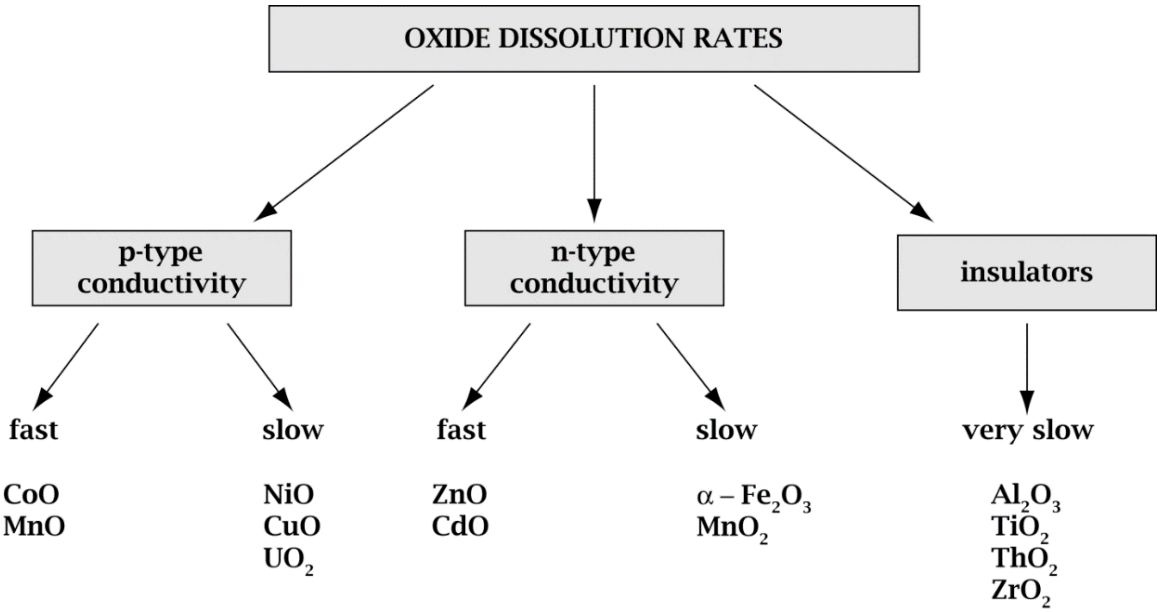

Figure 10: Categorization of the dissolution rates of various oxides separated according to their conductivity type (Segall et al. 1988).

8.1 PASSIVE CORROSION

Segall et al. (1988) have categorized oxides according to their conductivity-type and other chemical properties, Figure 10.

According to this categorization, ZrO_2, like TiO_2, belongs to the insulating oxide category and should dissolve very slowly in acidic, and especially neutral, solutions. Dissolution involves coordination of the metal cation in the surface of the oxide by OH^- leading to hydrolysis prior to the breaking of the strong M-O bond and transfer of the hydrolyzed cation ($Zr(OH)_5^-$ in the case of ZrO_2) into solution (Segall et al. 2010). For this reason these oxides are more soluble in (section 7), and hence more likely to dissolve in alkaline solutions, albeit very slowly.

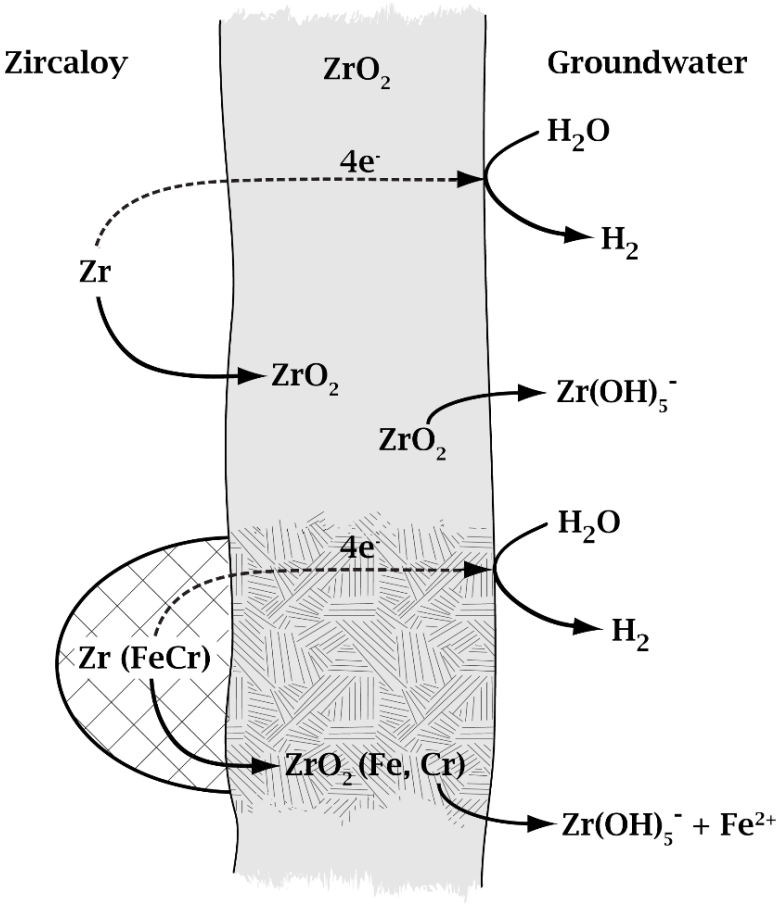

Figure 11: Schematic illustrating the passive corrosion process occurring on a Zr alloy surface. The passive corrosion process involves a steady-state between the rate of chemical dissolution of the oxide at the oxide/groundwater interface and the rate of its regeneration by metal oxidation at the alloy/oxide interface. This requires electron transfer through the oxide to reduce H_2O. Since the oxide associated with corroded SPPs (Zr (Fe, Cr)) could have different properties to that associated with the Zircaloy matrix, the passive corrosion process may temporarily proceed at a different rate at locations involving SPPs.

The dissolution process is insensitive to redox conditions since Zr is unstable in alternative oxidation states to that (Zr^{IV}) existing in the oxide, and cannot, therefore, be converted to more soluble states. This is in contrast to Fe oxides (e.g., Fe_2O_3) which are insoluble in the Fe^{III} state, but considerably more soluble when reduced to Fe^{II}, Figure 10, and UO_2 which is many orders of magnitude more soluble when oxidized from the U^{IV} state to the U^{VI} state (as UO_2^{2+}) (Grenthe et al. 1992; Guillamont et al. 2003).

When the oxide is present as a passivating layer on Zr and its alloys, its dissolution will not lead to further metal/alloy corrosion unless a passive corrosion process can be sustained. Such a process involves a balance between the chemical dissolution rate of the oxide at the oxide/solution interface and the metal oxidation (corrosion) process required to regenerate the oxide at the alloy/oxide interface, as illustrated schematically for Zr/ZrO_2 in Figure 11.

Since ZrO_2 is an insulator, such a balance could only be established across a very thin or highly defective (see below) oxide layer, since electron transfer to reduce H_2O, Figure 11, is required to balance metal oxidation at the alloy/oxide interface. Since the CANDU cladding discharged from reactor will be covered by an oxide ~5 µm in thickness (and thicker for BWR cladding) (section 3), a considerable extent of oxide dissolution should be required before the conditions for passive corrosion can be established. However, it should be noted that there is no confirmed evidence for a passivating barrier layer under the aggressive in-reactor conditions (section 3), the absence of which would allow access of H_2O to the alloy/oxide interface. However, under the non-aggressive wet storage conditions in reactor IFBs, a barrier layer would be expected to form at porous locations in the cladding oxide. While it can be realistically expected that the thick cladding oxide will provide substantial protection against passive corrosion under DGR conditions, the worst-case scenario would be that this process is limited only by the thin barrier layer present at the base of pores in the cladding oxide; i.e., corrosion proceeds at the rate established at the surface of the barrier layer at the base of pores. Given the extremely low solubility of crystalline ZrO_2 (Figures 8 and 9) in the neutral groundwater conditions anticipated in a Canadian DGR, a meaningful rate of passive corrosion seems very unlikely (see below).

A considerable data base of passive corrosion rates exists for Ti alloys. These studies show the dissolution rate is dependent on the point defect density in the oxide and the creation of surface states that can be neutralized by transfer to solution (Hua et al. 2005). That the rate of oxide dissolution is dependent on defect density was clearly demonstrated for NiO (which is also redox-insensitive), the rate differing by two orders of magnitude depending on the method of preparation and the subsequent defect annealing temperature employed (Jones et al. 1977; Pease et al. 1986).

While TiO_2 and ZrO_2 are not in the same oxide category as NiO (Figure 10), a similar, but independently developed, understanding of the passive corrosion of Ti has been published (Hurlen and Hornkjol 1991). It was claimed that passive corrosion of Ti in neutral solutions was controlled by the migration of the prominent defect (an O_V) in the oxide. Since transport in ZrO_2 also involves O_Vs (section 3), a similar passive corrosion mechanism should prevail. Since the oxide growth process also utilizes point defects (Macdonald 1999), their number density and, hence, their subsequent influence on the oxide dissolution process, are strongly influenced by the mode of preparation of the oxide.

Oxides grown slowly on Ti and shown to possess a low defect density (Blackwood and Peter 1990), dissolved much more slowly than those with a large defect density caused by their rapid growth. In addition, with exposure time to the aqueous environment, TiO_2 films initially grown

rapidly (and hence defective) underwent a defect annealing process which eventually rendered them inert to dissolution. Such a defect annealing process has been demonstrated electrochemically for both TiO_2 films (Leitner et al. 1986) and for the oxide films on Zr, Zr-2 and Zr-Nb alloys (Jensen 2002).

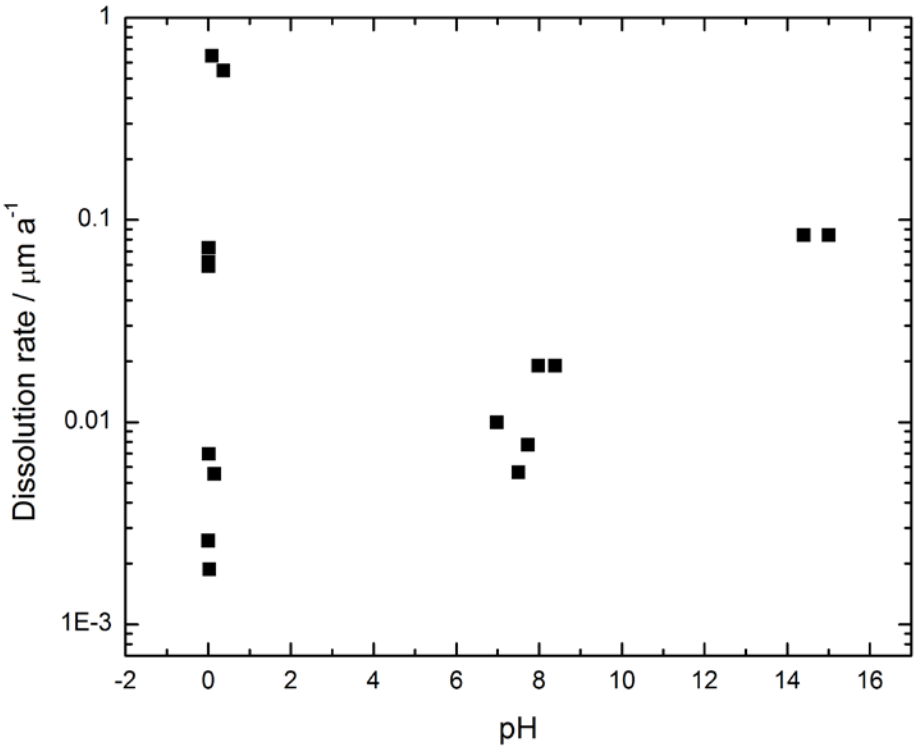

Figure 12: Dissolution (passive corrosion) rates of anodically grown oxides on Zr as a function of pH (Mogoda 1999a; El-Mahdy and Mahmoud 1998; El-Mahdy et al. 1996; Huot 1992; Allah et al. 1989).

Attempts to measure passive corrosion rates on Zr covered by ZrO_2 have been made (Magoda 1999a, 1999b; El-Mahdy and Mahmoud 1998; El-Mahdy et al. 1996; Huot 1992; Allah et al. 1989; Mogoda 1999). As noted above the rates depend on the conditions of preparation which control the defect density in the oxide. Passive corrosion rates were determined using capacitance measurements to determine the change in oxide film thickness with time. Films grown in this manner consist of two layers; an outer hydroxide or hydrated ZrO_2 layer which dissolves more rapidly than an inner barrier layer which possesses properties more closely resembling those expected of a stable passive oxide layer. Figure 12 shows attempted measurements of the rates of the inner layer.

The irreproducibility of the rates calculated in acidic solutions shows the variability generated by differences in defect density and emphasizes the difficulties in making laboratory measurements relevant to the behaviour of thick well-crystallized oxides on cladding. Even allowing for such ambiguities over film properties, the passive corrosion rates measured in neutral solutions are in the range 5 to 20 nm/a and must be considered both conservative and uncertain. The uncertainty arises partly from the need to adopt a value for the oxide dielectric constant, a parameter also strongly influenced by defect density, in order to convert capacitance into oxide

thickness. Since titanium alloys were proposed as corrosion barrier materials in the USA Yucca Mountain project and as a possible waste container material in other national waste disposal programs, its passive corrosion has been extensively studied (Johnson et al. 1994; Hua et al. 2004, 2005; Smailos et al. 1986, 1987; Shoesmith 2006). Some additional detail is included in Appendix B.

A number of attempts have been made to measure ZrO_2 film dissolution rates, equivalent to a corrosion rate if the steady-state illustrated in Figure 11 has been established. These short term studies (2–12 weeks) commonly conducted at high temperatures (≥250°C) mainly in alkaline solutions (pH from 11.8 to 13.5) when the solubility of Zr^{IV} is higher than in neutral solutions, yielded values between 0.1 µm/a and 0.4 µm/a (Gras 2014). In comparative studies the behaviour of Zr-4 (CANDU cladding) and Zr-2 (BWR cladding) were effectively the same. Experiments conducted at 25°C led to a rate <1 nm/a (Gras 2014, Table 13). In experiments on oxides (as opposed to oxide films on alloy surfaces) Curti (2002) noted that, as expected based on the discussion above, significantly lower dissolution rates were obtained for crystalline oxides compared to rapidly formed amorphous oxides/hydroxides. Based on the values in this range of measurements, Gras (2014) proposed an oxide dissolution (corrosion) rate of ~1 nm/a.

As noted above for electrochemical measurements, it is also difficult to make meaningful measurements of corrosion rates based on weight change. For this reason, high temperature growth laws, developed empirically, have been used in attempts to determine rates by extrapolation to DGR temperatures. The model parameters derived for these growth laws are listed by Gras (2014, Table 19). Hillner (1998, 2000) summarized and revised these models to develop optimized laws which could be extrapolated, an approach, which was updated and used in the USDOE Yucca Mountain project (Bale 2000). Only minimal passive corrosion of cladding was predicted, consistent with the observations that no observable cladding corrosion is observed on fuel elements under IRF conditions (section 5).

The approach used in these studies assumes the cladding is in the post transition condition although it is unclear that the porosity inherent to the oxide on cladding under in-reactor conditions will be maintained after the extended exposure to wet conditions in the IRF. It is likely the porosity will be resealed by the formation of a thin barrier layer at the base of the pores. With few exceptions, attempts to measure passive corrosion rates on Zircaloys at low temperatures have inevitably been conducted on freshly prepared specimens covered only by an air-formed native oxide and are, therefore, measurements of corrosion rates in the pre-transition region. Under these conditions, film growth will be initially rapid with the rate decreasing with time. Additionally, the oxide will not be equivalent to those formed under extended in-reactor exposure. Performing experiments for a duration long enough to achieve a post-transition state is unrealistic and the achievement of such a state is very unlikely to ever occur at low temperature film growth rates.

In attempts to obtain reliable pre-transition rates at temperatures relevant to those expected in a DGR, the extent of H production has been used (Kurashige et al. 1999; Wada et al. 1999). As expected, corrosion rates were initially high and decreased with time as oxide formation progressed. Since only the amount of H_2 evolved and not the amount absorbed into the alloy was measured, the rates cannot be considered quantitatively reliable.

A more thorough study was conducted by Kato et al. (2013), who measured both evolved and absorbed H on Zr-4 exposed to H_2O and alkaline solutions (pH = 12.5) over a period of 2 years. While rates decreased with time as oxide growth progressed, attempts to fit the rates to the cubic law determined from high temperature measurements (Tanabi et al.2013) were not totally

successful, the measured rates being higher. This is not surprising since the thin oxide grown over a short exposure period at low temperatures will not exhibit identical properties to that grown at high temperatures. Despite these inconsistencies, rates estimated using the data of Kato (2013) yielded rates ranging from 3 to 11 nm/a which are similar to those adopted by various national programs which range from 1 to 10 nm/a (Rothman 1984; Johnson and McGinnes 2002; SKB 1999; SKB 2006; Shoesmith and Zagidulin 2011).

Similar experiments conducted by Sakuragi (2012), some of which extended to 3 to 5 years, yielded similar corrosion rates which, while decreasing with time, also did not closely fit the model predictions of Hillner (1998, 2000). While no influence of the alloy (Zr-2 or Zr-4) was observed, the rates in alkaline solutions were slightly higher than in H_2O which could reflect the greater solubility of the oxide under alkaline conditions. Accompanying H absorption measurements showed that ~90% of the H produced was absorbed into the metal/alloy irrespective of either the material (Zr, Zr-2, Zr-4) or the pH (~ neutral to 12.5). The fraction of H absorbed did not change as the corrosion rate decreased indicating that the oxide formed did not become impermeable to H as it grew.

This high absorbed fraction raises the question of the specific mechanism of H absorption. Under high temperature conditions the fraction absorbed increases after the transition in oxide properties (Figure 1) (Motta et al. 2015) suggesting that the process could be supported by access of H_2O to the alloy/oxide interface, via grain boundaries or pores in the oxide, where it is reduced to absorbable H in support of further Zr oxidation. While this would be consistent with neutron reflectometry observations (Appendix A), it does not unequivocably confirm this is the dominant route for the on-going absorption observed by Sakuragi (2012), which was observed on a thin pre-transition oxide at low temperatures.

Based on claims that H enters the oxide as H^+ (Cox and Wong 1999), Motta et al. (2015) envisaged the film growth process involving a counterbalancing flow of O_V and H^+ in the electric field across the growing oxide with the elimination of O_V at the oxide/solution interface accompanied by H^+ reduction, leading to absorbable H, at the alloy/oxide interface.

Although the relative importance of these two possible mechanisms remains undefined, the second mechanism would require the oxidation/H absorption process to be transport limited with properties such as the electronic conductivity of the oxide playing a key role (Couet et al. 2014a; Motta et al. 2015). Irrespective of the actual mechanism, which intuitively seems unsustainable as the oxide thickens, the available data indicates a conservative maximum corrosion rate of 1 to 5 nm/a over a long exposure period. Based on these values, and the uncertainties associated with them, a slow hydriding of the cladding cannot be ruled out under DGR conditions. The estimated lifetime of the cladding would be in the region of 10^5 years (Gras 2014). Such a lifetime can be considered a conservatively short estimate for a number of reasons:

1. The values were measured over relatively short exposure periods when the oxides formed would be thin and defective.
2. The potential influence of the thick cladding oxide grown in-reactor is not taken into consideration. It is unlikely that H transport through an oxide a few microns thick will be as extensive as that through the thin (few nanometres) thick oxide present in the experiments described.
3. Even if the oxide on the cladding remained in the post-transition state (i.e., porous) allowing access of groundwater to the alloy/oxide interface, which seems unlikely, the available exposed alloy surface available to support corrosion would be significantly limited.

4. If it was necessary to remove the cladding oxide by chemical dissolution to establish the passive condition allowing H absorption under the conditions illustrated in Figure 11, a minimum of a few thousand additional years would be required to establish H absorption conditions. Given the crystalline nature of the oxide and the extremely low dissolution rates anticipated, this induction period is likely to be much longer.

The groundwater anion with the most potential to influence the passive corrosion of Zr is F^- which increases the solubility of Zr^{IV} (section 7) and can accelerate corrosion even when present at low concentrations (Pinard-Legry et al. 1989; Bale 2000) although, it has been claimed that F^- can actually inhibit corrosion (Yau and Maguire 1990). The influence of TiO_2 film properties in resisting corrosion in F^- solutions has been reviewed (Hua et al. 2005) including in dental implant studies when exposure to F^--containing solutions is common (Lorenzo de Melo and Cortizo 2000). When present at a sufficient [F^-] (≥1 mM) in acidic solutions (Kong 2008; Marici et al. 2014), F^- can be intercalated into the oxide using O_V sites leading to enhanced oxide dissolution and the eventual breakdown of the oxide film introducing the possibility of localized corrosion. However, while the aggressiveness of F^- in acidic solutions is well characterized (Mandry and Rosenblatt 1972; Wilhelmsen and Grande 1987; Kong 2008) no influence on passivity was observed at pH = 6.5 if an oxide had been preformed (Lorenzo de Melo and Cortizo 2000). These observations are consistent with those of Yau (2005) who noted, based on a literature review, that F^-, present at sub-millimolar levels in groundwater had no observable effect on Zr corrosion. The elimination of O_Vs in oxides on both Ti and Zr has been shown to substantially suppress oxide dissolution rates on Ti, and by analogy on Zr (Pan et al. 1997; Blackwood et al. 1988; Choi et al. 1992). These results are consistent with the observations of Yao and Sutherlin (2005) who noted, based on a literature review, that F^- present at sub-millimolar levels in groundwater had no observable effect on the passive corrosion of Zr. Given the many years of thermal annealing of cladding oxides under dry storage conditions (section 5), the neutral pH in a Canadian DGR, and the minimal [F^-] in groundwater (~2 ppm; Table 2), this anion should exert a negligible effect on the passive corrosion of the cladding.

Studies on the influence of F^- on the properties of oxide films on titanium, with similar behaviour anticipated for Zr, showed the ability of F^- to influence oxide properties decreased as the oxide thickness increased (Kong 2008; Mareci et al. 2014). A more detailed review of the influence of F^- on the properties of TiO_2 showed that if F^- was to influence the corrosion properties of Ti (and by analogy, Zr) it would be by causing localized oxide film breakdown leading to the initiation of pitting (Hua et al. 2005). Given the thickness of oxide films on Zircaloy cladding (~5 µm on CANDU fuel and 30 to 50 µm on BWR fuel), which are orders of magnitude thicker than those possible in low-temperature laboratory experiments, the many years of thermal annealing, and the low [F^-] expected in groundwater, any influence on localized corrosion would be negligible especially in the presence of large [Cl^-] (Table 2).

8.2 LOCALIZED CORROSION

As noted in Appendix A the electrochemical polarization of Ti and Zr and their alloys to more positive potentials, a treatment which simulates the establishment of more oxidizing conditions under open circuit (corrosion) conditions, produces different results which are summarized in Figure 13.

The passive film on Ti and its alloys is more resilient under anodic (oxidizing) conditions while that on Zr and its alloys is more resilient under cathodic (reducing) conditions. As described in

Appendix A, while the film growth mechanisms for both metals may be the same, the physical properties of the oxides are different. For Zr, stress-induced film crystallization leads to the introduction of pathways, most likely grain boundaries or pores, which allow access of H_2O and the migration of ionic species to the alloy/oxide interface (Cox 1970; Leach and Pearson 1988; Ortega and Siejka 1982). For Ti, the oxide film remains amorphous and undergoes potential-induced crystallization only at high potentials (Shibata and Zhu 1995) unattainable under natural corrosion conditions.

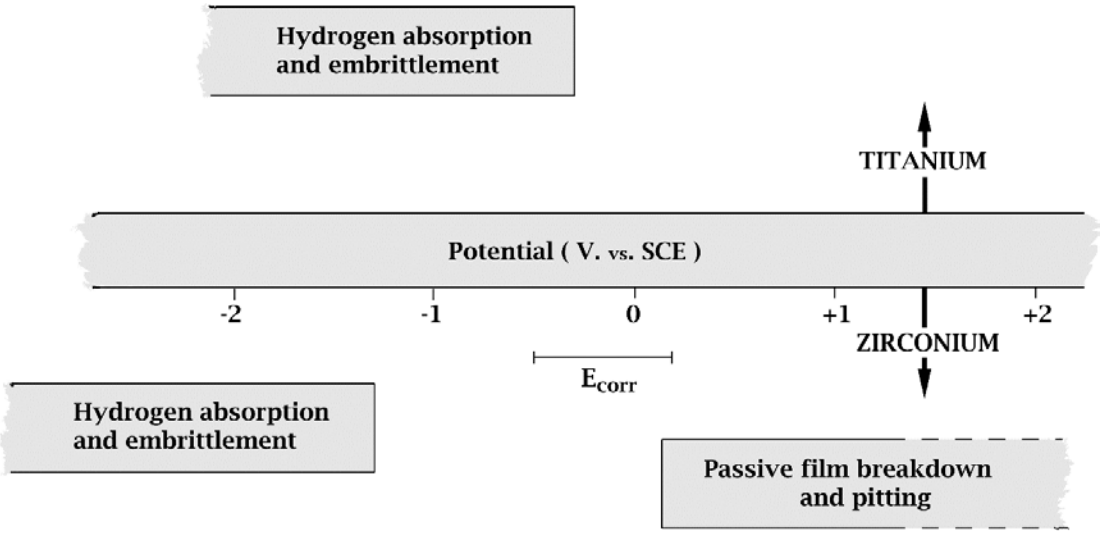

Figure 13: Schematic showing the potential ranges within which passive film breakdown/pitting and H absorption/embrittlement could occur on Ti and Zr alloys. The bar marked E_{CORR}, shows the range of corrosion potentials measured on Zr alloys in neutral solution.

The localized corrosion properties of Ti alloys have been reviewed in detail (Hua et al. 2004, 2005; Shoesmith and Ikeda 1997) and show, as expected based on these film properties, an excellent resistance to pitting under oxidizing conditions. Pitting breakdown potentials (E_{RP}) for the α-phase alloys are in excess of 7 V, and even for β-phase containing alloys are in the region of 2 V (Shoesmith and Ikeda 1997), potentials unachievable under natural corrosion conditions.

For Zr and its alloys, the availability of migration pathways leads to values of E_{Pit} and E_{RP} (defined below and in Figure 14) which are considerably lower. Consequently, many studies of Zr alloy susceptibility to pitting have been reported (Meisterjahn et al. 1987; Mamun et al. 2001; Knittel et al. 1982; Greene et al. 2000; Fahey et al. 1997; Hornkjoel 1988; Maguire 1984; Mankowski et al. 1989; Satpati et al. 2005; Knittel and Bronson 1984; Pourbaix 1970; Brossia et al. 2000; Pan et al. 2001; Gras 2014). These studies generally utilized the standard potentiodynamic polarization method in which the potential applied is scanned to positive values (simulating increasingly oxidizing conditions) until the pitting breakdown potential (E_{Pit}) is surpassed, and then back again until the repassivation potential (E_{RP}) is achieved, as illustrated in Figure 14.

Based on the application of this technique, Zr alloys would be classified as more susceptible to pitting compared to Ti and its alloys providing the [Cl^-] is high, Figure 15 (Knittel and Bronson 1984; Jangg et al. 1978), which could be the case in a Canadian DGR (Table 2). Additional

investigations show a similar film breakdown in Br^- and I^- solutions, although at much higher potentials (Hornkjoel 1988).

Comparison of E_{Pit} values determined in this manner to E_{CORR} values from a range of studies (Gras, Hornkjoel 1988) (shown as a horizontal line in Figure 13) suggests that Zircaloy cladding could be susceptible to pitting providing conditions were sufficiently oxidizing (i.e., E_{CORR} values were in the range in which the horizontal bar in Figure 13 overlaps the range within which breakdown/pitting can occur). If susceptibilities were to be based on E_{RP}, a commonly used and very conservative approach in corrosion engineering, then pitting would be classed as more likely since values more negative than the E_{CORR} range shown in Figure 13 have been reported (Bellanger and Rameau 2000; Gardiazabal et al. 1981; Gomez et al. 1985; Chen et al. 1985; Galvele et al. 1990) although values summarized in Gras (2014) indicate this should only occur for pH<3 in dilute Cl^- solutions even with H_2O_2 present.

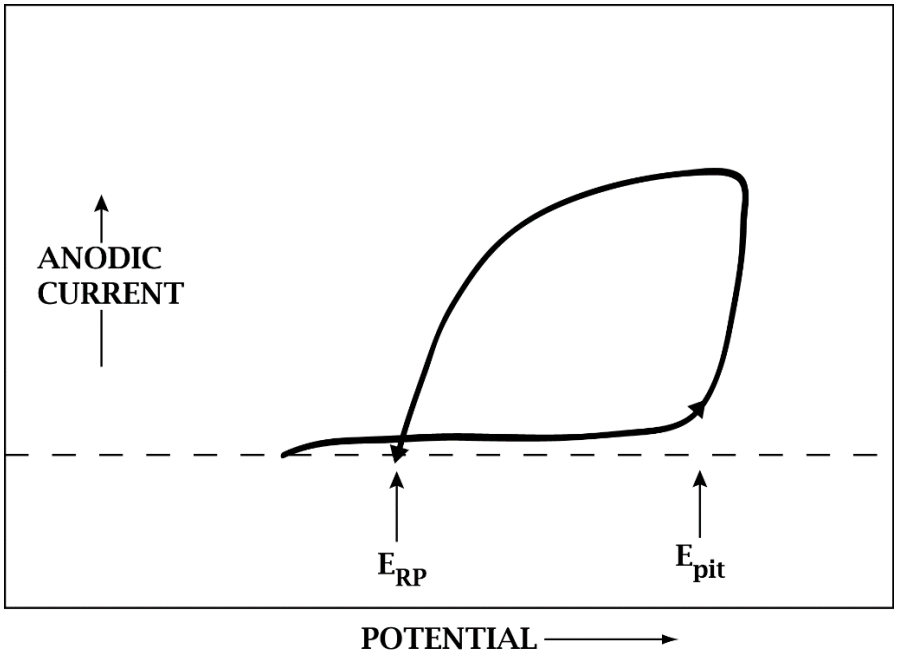

Figure 14: Illustration showing the form of the current-potential relationship observed in a potentiodynamic scan recorded to determine the pitting breakdown potential (E_{Pit}) and the repassivation potential (E_{RP}).

However, the application of the potentiodynamic technique to Zr alloys has many issues and, as noted by Gras (2014) and Shoesmith and Zagidulin (2011), can produce results at odds with those based on corrosion experiments and industrial experience. Generally, experiments to determine susceptibilities are performed on freshly prepared alloy surfaces covered, at best, by a highly defective oxide not representative of the oxide present on cladding surfaces on discharge from reactor. Additionally, the application of a potential scan even at the slow rate commonly employed (0.167 mV/s) leads to the further growth of defective oxide and the introduction of the oxide/alloy interfacial stresses which promote pit initiation. Under natural corrosion conditions, film growth would be considerably slower and accompanied by defect annealing, and pit initiation avoided.

Additionally, the presence of a pre-grown oxide led to an increase in the pitting breakdown potential for Zr-4 measured in a millimolar Cl^- solution to 600 mV (vs SCE), a value >800 mV more positive than values recorded on a freshly prepared surface. Values of E_{Pit} were found insensitive to pH over the range 8 to 12 (Lavigne et al. 2012). A similar increase in E_{pit} was observed on Zr-4 exposed to dilute Cl^- solutions at 95°C (Brossia et al. 2000; Pan et al. 2001).

Based on these studies the two key requirements for pitting to occur are a high [Cl^-] and conditions sufficiently oxidizing to drive E_{CORR} to values >E_{pit} (i.e., into the potential region labelled "Passive film breakdown and pitting" in Figure 13). Experiments summarized by Gras (2014) showed this did not occur even in the presence of H_2O_2 (added to simulate radiolysis products), results consistent with those of Maguire (1984) who reported that very strong oxidants, such as $Fe^{3+}/Cu^{2+}/Cl_2$ were necessary to cause pitting. Since both Fe and Cu from container corrosion will only be present in the reduced form (Fe^{2+}, Cu^+) and the pH only slightly acidic or neutral (Colás et al. 2021, 2022; Hall et al. 2021) their ability to induce pitting will be negligible (Yau 2005; Yau and Sutherlin 2005). In support of these arguments (Kurashige 1999) observed no pitting on Zr-4 at 30°C to 45°C in anoxic slightly alkaline (pH = 10.5) to alkaline solutions containing 0.55 M Cl^- over an exposure period of up to 500 days under natural corrosion conditions.

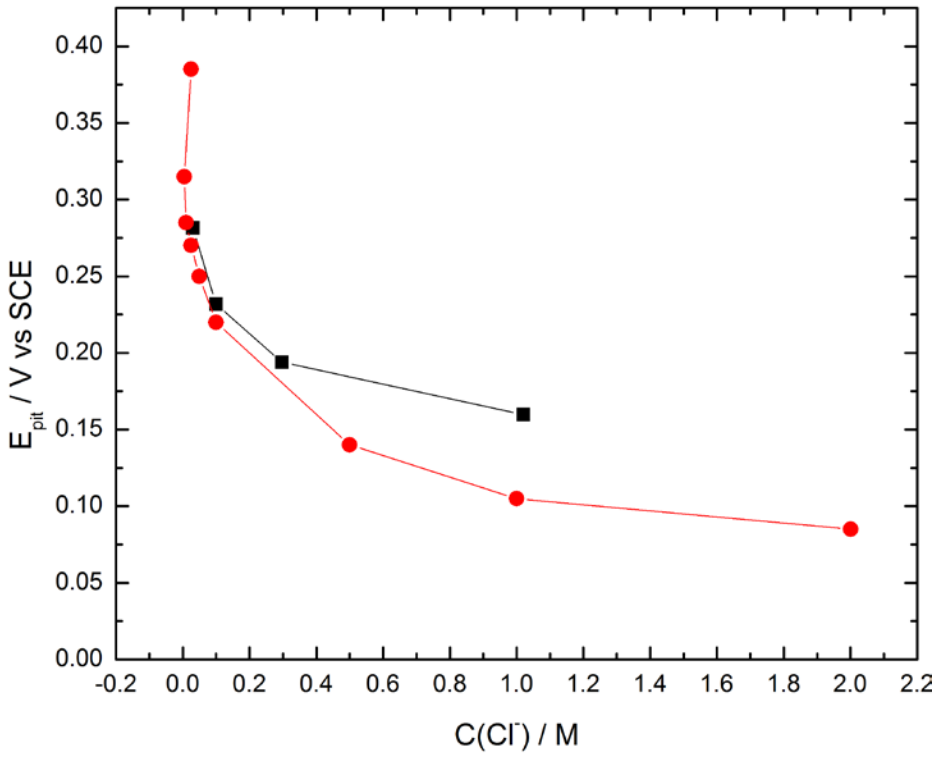

Figure 15: Pitting breakdown potentials recorded on freshly polished Zr surfaces after allowing the E_{CORR} to achieve a steady0state value (i.e., on surfaces covered by only a thin surface oxide film) as a function chloride concentration (C); ○-Knittel and Bronson (1984); □ Jangg et al. (1978).

9. THE INFLUENCE OF RADIATION

Providing container failure does not occur at short emplacement times when radiolysis of humid air would be possible (as discussed in section 6.1), the only source of oxidants will be those produced by the radiolysis of H_2O of which only the molecular oxidant H_2O_2 would have any significant influence on materials corrosion processes beyond the surface of the fuel. Providing containment preventing access of groundwater to the cladding surface is maintained for $\geq 10^3$ years, γ-radiation dose rates at the cladding surfaces will be $\leq 10^{-3}$ Gy/h and $[H_2O_2]$ some orders of magnitude below the micromolar level, and, thus, expected to exert a negligible influence on cladding corrosion.

This claim that radiolysis will exert a negligible influence on Zr alloy corrosion is supported by a wealth of evidence on radiation effects on the corrosion of passive materials (Shoesmith and King 1999; Landolt et al. 2008; Farnan 2019). While little data exists for Zr alloys, Ti and its alloys have been well studied. No significant influence of γ-radiation was observed on a number of Ti alloys in a wide range of environments including Mg-containing saturated brines at temperatures up to 250 ^oC, conditions considerably more aggressive than even the most concentrated sedimentary rock groundwater (Table 2). Gamma dose rates in the region of 10^3 Gy/h did lead to increased corrosion rates and the incorporation of groundwater species, such as Mg^{2+}, into the outer regions of the passive film, but such dose rates are well in excess of the highest values possible on the outer cladding surface (as noted in section 6.1).

There is evidence to show that radiation exposure decreases the susceptibility to localized corrosion on both Zr-4 (Bellanger and Rameau 2000) and Ti (Ikeda et al. 1990). A dose rate of ~10^2 Gy/h was shown to inhibit the propagation of crevice corrosion on commercially pure Ti (Grade-2) (Ikeda et al. 1990) which is known to be susceptible to this form of corrosion under the conditions tested (Noël et al. 2001). Since crevice corrosion can initiate and propagate on Ti by a similar mechanism to that for the pitting of Zr alloys and at potentials considerably lower than the measured E_{CORR} values for Zr alloys, a similar influence of radiation on the pitting of cladding would be anticipated. For localized corrosion to occur, anodic (metal dissolution) and cathodic (oxidant reduction) sites must be separated on the corroding surface (in an electrochemical experiment they are artificially separated on different electrodes). By producing oxidants universally across the surface, γ-radiation could prevent the stable maintenance of such separated locations.

Experiments which attempt to simulate radiation effects by the chemical addition of H_2O_2 detect slightly enhanced corrosion of Ti alloys (Pan et al. 1994; Pan et al. 1996; Kim and Oriani 1987a, 1987b; Zhang 2017). For Ti alloys, in neutral H_2O_2 solutions with millimolar concentrations (commonly phosphate buffered solutions used to simulate the in-vivo conditions experienced by body-implants), the corrosion resistance was decreased leading to thickening of the surface oxide film. The film was comprised of an inner barrier layer and an outer more porous layer which X-ray photoelectron spectroscopy demonstrated contained a high OH^- content. Since the specimens used in these experiments were freshly polished prior to solution exposure, initially higher corrosion rates were generally found to decrease with time as films thickened and their defect concentration decreased. The slightly enhanced corrosion rates and thicker films were attributed to the redox sensitivity of Ti and its ability to form Ti-H_2O_2 complexes (Tengvall et al. 1989a, 1989b) which are subsequently hydrolyzed leading to the high OH^- content of the outer layers of the surface film. This has been more extensively demonstrated in more alkaline solutions (pH≥10) in which the formation of metastable complexes ($Ti(OH)_2O_2$) have been shown to form (Been and Tromans 2000; Rämo et al. 2002).

By contrast the redox insensitive ZrO_2 film on Zr alloys does not lead to observable enhanced corrosion in H_2O_2 solutions (Zhang 2017), with the peroxide readily undergoing decomposition catalyzed on the redox-inert ZrO_2 surface via a radical process (Xiao et al. 2010; Hiroki and LaVerne 2005; Lousada et al. 2010; Lousada et al. 2013),

$$H_2O_2 \rightarrow 2OH^{\bullet} \quad (11)$$

$$OH^{\bullet} + H_2O_2 \rightarrow HO_2^{\bullet} + H_2O \quad (12)$$

$$2HO_2^{\bullet} \rightarrow H_2O_2 + O_2 \quad (13)$$

In these studies, no measurable influence of H_2O_2 even on Ti alloy corrosion, was observed for $[H_2O_2]<5\times10^{-5}$ M. At the low radiation dose rates prevailing at the inner and outer cladding surfaces, the $[H_2O_2]$ will be many orders of magnitude lower than this. This, and the considerable concentrations of the oxidant scavengers Fe^{2+} and H_2 produced by the corrosion of the steel container vessel, will render any influence of radiolytic oxidants on cladding corrosion negligible.

Figure 16 summarizes the influence of γ-radiation on a series of materials studied in a range of neutral saline environments (up to $[Cl^-]$ = 34,000 mg/L which is similar to those anticipated in a crystalline rock DGR (Table 2)). Even if Zr alloys were to perform no better than the much more susceptible stainless steels, no significant effect of radiation would be observed beyond a few

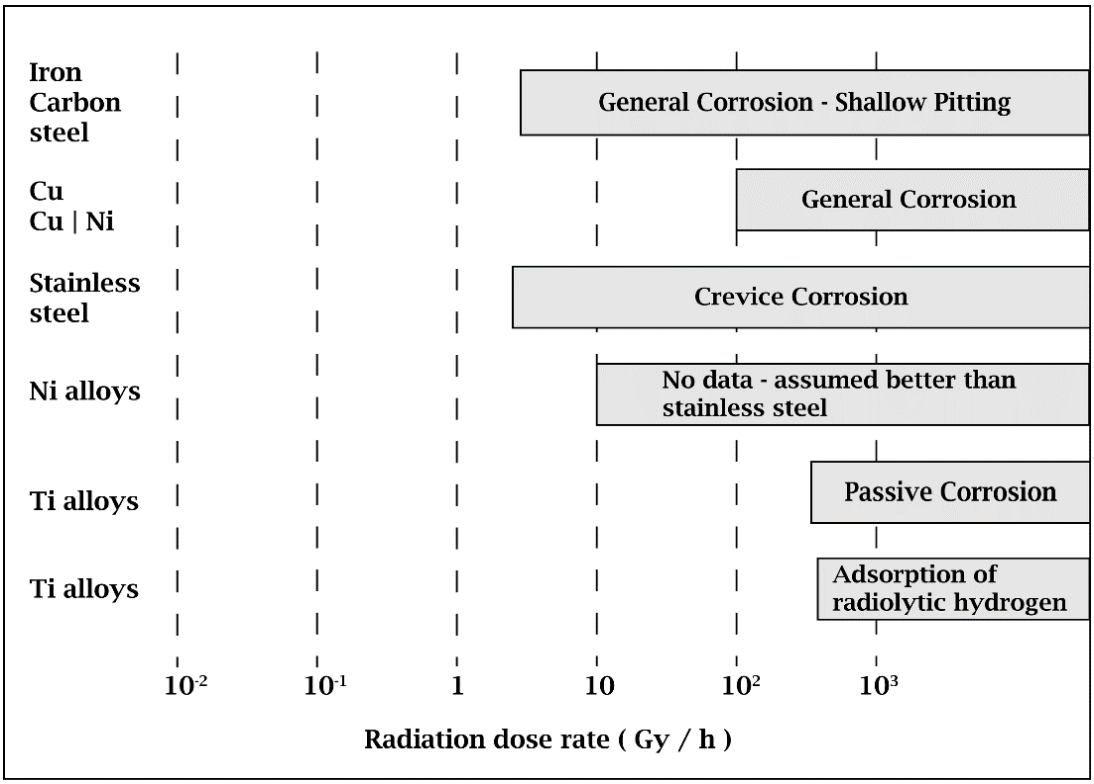

Figure 16: Summary showing the gamma radiation dose rate ranges (shaded areas) within which a measurable influence of radiation on various corrosion processes on

various materials has been observed (Shoesmith and King 1999). At dose rates below these regions experiments have revealed no observable radiation effect.

hundred years of disposal in a DGR, Figure 6, a period well before containers would be expected to fail and allow contact of groundwater with the cladding. This claim is supported by the results of Verlet [2015] who observed no measurable influence of H_2O radiolysis on the corrosion of the Zr-4 and M5™ alloys.

10. SUMMARY AND CONCLUSIONS.

The degradation and corrosion of Zr alloy nuclear cladding has been reviewed under wet and dry storage conditions and under the permanent disposal conditions anticipated in a Canadian deep geologic repository.

Under storage conditions, most possible degradation processes will not be operative. The one possible exception is DHC at the assembly welds, which can also be ruled out despite the presence of substantial hydride levels in the cladding on discharge from reactor. A combination of experiments and model calculations show that, while H levels will be higher than the terminal solubility and hydrides will be present, the stress intensity factor which could develop will be well below the critical value required for crack propagation to failure for both CANDU and BWR cladding.

Under DGR conditions, the potential corrosion/degradation behaviour has been analyzed based on a comprehensive review of the in-reactor oxide growth and hydrogen absorption processes. While the emphasis was predominantly on CANDU reactor cladding (Zr-4), comparisons to the anticipated behaviour on BWR cladding (predominantly Zr-2) is also referred to. Also, since the corrosion properties of Zr exhibit similarities and instructive differences to those of Ti, the behaviour of the two materials is compared when possible.

Of the possible degradation modes only general passive corrosion, possibly accompanied by H absorption leading to hydride formation is feasible. While the pitting of Zr alloys may be feasible within the corrosion potential range possible in a DGR, especially a Canadian DGR where the chloride concentrations could be high, the absence of oxidants such as groundwater oxygen and the extremely low hydrogen peroxide concentrations produced by water radiolysis means pit initiation and propagation can be considered negligible.

Passive corrosion will be driven either by the extremely low dissolution rate of the oxide layer on the cladding surface or by reaction of the alloy with groundwater at the base of pores in the cladding. Neither of these two possible processes is sensitive to the groundwater composition. The concentrations of F^-, potentially the most reactive groundwater species, are expected to be very low and unaggressive at the neutral pH values anticipated. No significant difference in corrosion properties and rates is expected for Zr-4 and Zr-2.

Available published measurements show that, even if protection by the thick oxide present on the cladding surface on discharge from reactor is not taken into account, the corrosion rate will be very low and can be conservatively set within the range 1 to 5 nm/a. It is likely actual rates will be considerably lower.

Since H absorption into the alloy can be observed at the low temperatures possible in a DGR, the possibility that cladding will eventually fail by hydriding cannot be discounted. This process, and how it might occur at temperatures relevant to DGR conditions, is presently only poorly defined, but can only occur at a rate dictated by the corrosion rate. Based on the conservative corrosion rates (above) times to failure should be 10^5 years or longer.

REFERENCES

Adamson, R., F. Garzarolli, B. Cox, A. Strasser and R. Rudling. 2007. Corrosion mechanisms in zirconium alloys. Advanced Nuclear Technology International Europe AB, October 2007.

Adamson, R., M. Griffiths and C. Paterson. 2017. Irradiation growth of zirconium alloys: a review. Ant International, Tollered, Sweden; December 2017 (www.antinternational.com).

Ahn, T.M. 2019. Delayed hydride cracking (DHC) of cladding materials: an analysis for storage and disposal of spent nuclear fuel. Nuclear Engineering and Design 350, 128-136.

Ai, J., Y. Chen, M. Urquidi-Macdonald and D.D. Macdonald. 2008. Electrochemical impedance spectroscopic study of passive zirconium. Journal of Nuclear Materials, 379, 162-168.

Allah, A.G., A.A. Mazhar, F.E.T. Heakal and M.A. Ameer. 1989. Formation and dissolution of anodic oxide films on zirconium in NaOH; Kinetic studies. Journal of Applied Electrochemistry, 19, 213-218.

Allen, T.D., R.J.M. Konings and A.T. Motta. 2012. Corrosion of zirconium alloys: Comprehensive Nuclear Materials; edited by R.J.M. Konings. 5, 49-68.

Andra. 2005. Référentiel du comportement des radionucléides et des toxiques chimiques d'un stockage dans le Callovo-Oxfordian jusqu'à l'homme. Tome 2. Andra Technical Report Dossier 2005, Réf. C.RP.ASCM.04.0032.A. Chapter 5, 41 (In French).

Ariani, I. 2022. Dose rate analysis to support radiolysis assessment of used CANDU fuel. Nuclear Waste Management Organization Report NWMO-TR-2022-02. Toronto, Canada.

Badley, M. and D.W. Shoesmith. 2022. The corrosion/dissolution of used nuclear fuel in a deep geological repository. Nuclear Waste Management Organization Report, NWMO-TR-2022-09. Toronto, Canada.

Baes, C.F. and R.E. Mesmer. 1976. The hydrolysis of cations. Wiley-Interscience, John Wiley and Sons, New York, USA.

Bale, M. 2000. Clad degradation – Local corrosion of zirconium and its alloys under repository conditions. USDOE – OCRWM Report ANL-EBS-MD-00012 REV00, March 2000.

Barb, W.G., J.H. Baxendale, P. George and K.R. Hargrave. 1951. Reactions of ferrous and ferric ions with H_2O_2. II The ferric reaction. Transactions of the Faraday Society, 47, 591-616.

Been, J. and D. Tromans. 2000. Titanium corrosion in alkaline hydrogen peroxide. Corrosion 56, 809-818.

Bellanger, G. and J.J. Rameau. 2000. Inhibition of chloride pitting corrosion of Zircaloy-4 alloy in highly radioactive water by radiolytic nitrate and hydrogen peroxide. Journal of Materials Science, 35, 1759-1771.

Blackwood, D.J. and L.M. Peter. 1990. Potential modulated reflectance spectroscopy of anodic oxide films on titanium. Electrochimica Acta, 35, 1073-1080.

Blackwood, D.J., L.M. Peter and D.E. Williams. 1988. Stability and open circuit breakdown of the passive film on titanium. Electrochimica Acta 33, 1143-1149.

Blackwood, D.J., C.C. Naish, N. Platts, K.J. Taylor and M.I. Thomas. 1995. The anaerobic corrosion of carbon steel in granite groundwater. Swedish Nuclear Fuel and Waste Management Company Technical Report, TR-95-03, Solna, Sweden.

Blat, M. and D. Noel. 1996. Detrimental role of hydrogen on the corrosion rate of zirconium alloys: In Zirconium in the Nuclear Industry, 11th International Symposium. ASTM STP 1295, 319-337.

Blat, M., L. Legras, D.Noel and H. Amanrich. 2000. Contribution to a better understanding of the detrimental role of hydrogen on the corrosion rate of Zircaloy-4 cladding materials; In Zirconium in the Nuclear Industry, 12th International Symposium. ASTM STP 1354, 563-591.

Boyle, C.H. and S.A. Meguid. 2015. Mechanical performance of integrally bonded copper coatings for long-term disposal of used nuclear fuel. Nuclear Engineering Design. 293, 403-412.

Bossis, Ph., D. Pêcheur, K. Hanifi, T. Thomazet and M. Blat. 2004. Comparison of the high burnup corrosion on M5 and low tin Zircaloy-4 alloys. 14th International Symposium on Zirconium in the Nuclear Industry, Stockholm, June 13-17, ASTM STP 1467, 494-525.

Bradley, E.R., W.J. Bailey, A.B. Johnson and L.M. Lowry. 1981. Examination of Zircaloy-clad spent fuel after extended pool storage. Pacific Northwest Laboratories Report PNL-3921, Richland, Washington, USA.

Brady, P.V. and B.D. Hanson. 2020. An updated analysis of clad degradation: spent fuel and waste disposition. Sandia National laboratory Report SAND2020-13018R.

Brendebach, B., M. Altmaier, J. Rothe, V. Neck and M.A. Denecke. 2007. EXAFS study of aqueous Zr^{IV} and Th^{IV} complexes in alkaline $CaCl_2$ solutions: $Ca_3[Zr(OH)_6]^{4+}$ and $Ca_4[Th(OH)_8]^{4+}$. Inorganic Chemistry. 46, 6804-6810.

Broczkowski, M, D. Zagidulin and D.W. Shoesmith. 2010. The role of dissolved hydrogen on the corrosion/dissolution of spent nuclear fuel; in Nuclear Energy and the Environment; American Chemical Society Proceedings, Vol. 1046, Chapter 2, 349-380.

Brossia, C.S., C.A. Greene, D.S. Dunn and G.A. Cragnolino. 2000. Effects of environmental and electrochemical factors on the localized corrosion of Zircaloy-4. NACE Corrosion Paper 2210, March 2000.

Bruno, J., E. Cera, J. de Pablo. L. Duro, S. Jordana and D.Savage. 1997. Determination of radionuclide solubility to be used in SR97. Uncertainties associated to calculated solubilities. Swedish Nuclear Fuel and Waste Management Company Technical Report TR-97-33, Solna, Sweden.

Byrne, T.P. and J. Freire-Canosa. 1988. Effects of hydrogen/deuterium migration, fast fracture, stress rupture and oxidation on the stability of CANDU fuel stored in a dry air environment. Ontario Hydro Research Division Report 84-188-K. Toronto, Canada.

Chen, J.S., A. Bronson and D.R. Knittel. 1985. Pitting corrosion on zirconium in KCl and KCl-H_2SO_4 solutions. Corrosion, 41, 438-445.

Chevalier, S., G. Strehl, J. Favergeon, F. Desserey, S. Weber and O. Hientz. 2003. Use of oxygen isotope to study the transport mechanism during high temperature oxide scale growth. Materials at High Temperature. 20, 253-259.

Choi, Y.-K., S.-S Seo, K.-H. Choi and S.-M. Park. 1992. Thin titanium dioxide film electrodes prepared by thermal oxidation. Journal Electrochemical Society. 39, 1803-1807.

Colás, E., A. Valls, D. Garcia and L. Duro. 2021. Radionuclide solubility calculation (Phase 1). Nuclear Waste Management Organization Report NWMO-TR-2021-02. Toronto, Canada.

Colás, E., O. Riba, A. Valls, D. Garcia and L. Duro. 2022. Radionuclide solubility calculations (Phase 2). Nuclear Waste Management Organization Report NWMO-TR-2022-11. Toronto, Canada.

Couet, A., A.T. Motta and R.J. Comstock. 2014a. Hydrogen pickup measurements in zirconium alloys: Relation to oxidation kinetics. Journal Nuclear Materials. 451, 1-13.

Couet, A., A.T. Motta and R.J. Comstock. 2014b. Effect of alloying elements on hydrogen pick-up in zirconium alloys: In Zirconium in the Nuclear Industry; 17th International Symposium ASTM STP 1543, 479-509.

Cox, B. 1968. A porosimeter for determining the size of flaws in zirconia or other insulating films “in-situ”. Journal Nuclear Materials. 27, 1-11.

Cox, B. 1969. Rate controlling process during the pretransition oxidation of zirconium alloys. Journal Nuclear Materials. 31, 48-66.

Cox, B. 1970. Factors affecting the growth of porous anodic oxide films on zirconium. Journal Electrochemical Society. 117, 654-663.

Cox, B. 1985. Assessment of PWR waterside corrosion models and data. EPRI Technical Report NP-4287, Electric Power Research Institute, Palo Alto, CA, USA.

Cox, B. and C. Roy. 1966. Transport of oxygen in oxide films on zirconium determined by the nuclear reaction $O^{17}(He^3,\alpha)O^{16}$. Electrochemical Technology 4, 121-127.

Cox. B. and J.P. Pemsler. 1968. Diffusion of oxygen in growing zirconia films. Journal Nuclear Materials. 28, 73-78.

Cox, B. 1976. Oxidation of zirconium and its alloys. In; Advances in corrosion science and technology; edited by M.G. Fontana and R.W. Staehle, Plenum Vol.5 173-391.

Cox, B. 1990. Some thoughts on the mechanism of in-reactor corrosion of zirconium. Journal Nuclear Materials. 170, 1-23.

Cox, B. and Y.M. Wong. 1999. A hydrogen uptake micro-mechanism for Zr alloys. Journal of Nuclear Materials 255, 250-262.

Curti, E. and W. Hummel. 1999. Modeling the solubility of zirconia in a repository for high-level radioactive waste. Journal Nuclear Materials. 274, 189-196.

Curti, E. and C. Degueldre. 2002. Solubility and hydrolysis of zirconium oxides: a review and supplemental data. Radiochimica Acta 90, 801-804.

Dali, Y., M.Tupin, P. Bossis and M. Pijolat. 2012. Corrosion kinetics under high pressure of steam of pure zirconium and zirconium alloys followed by in-situ thermogravimetry. Journal Nuclear Materials. 426, 148-159.

Degueldre, C., J. Raabe, G. Kuri and S. Abolhassani. 2008. Zircaloy-2 secondary phase precipitate analysis by X-ray microspectroscopy. Talanta 75, 402-406.

Dollins, G.C. and M. Jursich. 1983. A model for the oxidation of zirconium-based alloys. Journal Nuclear Materials. 113, 19-24.

Electric Power Research Institute (EPRI). 2020. Phenomena identification and ranking table (PIRT) exercise for used fuel cladding performance. Report No. 3002018439. Palo Alto, CA. USA.

El-Madhy, G.A. and S.S. Mahmoud. 1998. Effect of different acid anions on the kinetics of the formation and dissolution behaviour of anodic zirconium oxide. Corrosion, 54, 354-361.

El-Mahdy, G.A., S.S. Mamoud and H.A. El-Dahan. 1996. Effect of halide ions on the formation and dissolution behaviour of zirconium oxide. Thin Solid Films, 286, 289-294.

Ensor, B., A.M. Lucente, M.J. Frederick, T. Sutliff and A.T. Motta. 2017. The role of hydrogen in zirconium alloy corrosion. Journal Nuclear Materials. 496, 301-312.

Eriksen, W.H. and D. Hardie. 1964. The influence of alloying elements on the terminal solubility of hydrogen in alpha zirconium. Journal Nuclear Materials. 13, 254-262.

Etoh, Y., S. Shimada. 1993. Neutron irradiation effects in intermetallic precipitates in Zircaloy as a function of fluence. Journal of Nuclear Materials. 200, 59-69.

Etoh, Y., S. Shimada and K. Kikuchi. 1992. Irradiation effects on corrosion resistance and microstructure of Zircaloy-4. Journal Nuclear Science and Technology 29, 1173-1183.

Fahey, J., D. Holmes and T-L. Yau. 1997. Evaluation of localized corrosion of zirconium in acidic chloride solutions. Corrosion, 53, 54-61.

Farnan, I., F. King, D. Roberts, V. Smith, S. Swanton, and R. Thetford. 2019. Effects of ionizing radiation on engineered barrier system performance. Wood Nuclear UK Limited, contractor report to UK Radioactive Waste Management, NDA Report No. RWM/Contr/19/041. Available from https://webarchive.nationalarchives.gov.uk/ukgwa/20200401140306/https://rwm.nda.gov.uk/publication/effects-of-ionising-radiation-on-engineered-barrier-system-performance/

Galvele, J.R., R.M. Torresi and R.M. Carranza. 1990. Passivity breakdown and its relation to pitting and stress corrosion cracking processes. Corrosion Science, 31, 563-571.

Gardiazabal, I., R. Schrebler and R. Cordova. 1981. The potentiodynamic behaviour of zirconium and Zircaloy-4 in chloride acid media. Journal of Electroanalytical Chemistry, 119, 389-394.

Garzarolli, F., D. Jorde, R. Manzel, G.W. Parry and P.G. Smerd. 1980. Review pf PWR fuel rod waterside corrosion behaviour. EPRI Technical report NP-1472, Palo Alto, Ca, USA.

Gobien, M., F. Garisto, E. Kremer and C. Medri. 2018. Seventh Case Study: Reference Data and Codes. Nuclear Waste Management Organization Technical Report NWMO-TR-2018-10. Toronto, Canada.

Godliewski, J., P. Bouvier, G. Lucazeau and L. Fayette. 2000. Role of intermetallic precipitates in hydrogen transport through oxide films on Zircaloy. In Zirconium in the Nuclear Industry; 12th International Symposium; ASTM STP 1354 877- 856.

Goldman, M., J.J. Noël and D.W. Shoesmith. 2020a. Long term sour corrosion of carbon steel in anoxic conditions. Corrosion, 76, 324-331.

Goldman, M., C. Tully, J.J. Noël and D.W. Shoesmith. 2020b. The influence of sulphide, bicarbonate and carbonate on the electrochemistry of carbon steel in slightly alkaline solutions. Corrosion Science, 169, 108607.

Gomez, H., J. Gardiazabal, R. Vera, E. Schrebler and R. Cordova. 1985. Passivation kinetics of Zircaloy-4 electrode in mineral acids under potentiodynamic conditions. Journal of Electroanalytical Chemistry 188, 39-48.

Gras, J.-M. 2014. State of the Art of ^{14}C in Zircaloy and Zr alloys – ^{14}C release from zirconium alloy hulls (D 3.1). European Commission CAST project, FP7, D3.1.

Greene, C.A., C.S. Brossia, D.S. Dunn, and G.A. Cragnolino. 2000. Environmental and electrochemical factors on the localized corrosion of Zircaloy-4. Corrosion 2000, Paper No. 002210. NACE International Annual Conference. Houston, Texas.

Grenthe, I., J.Fuger, R.J. Konings, R.J. Lemire, A.B. Muller, C. Nguyen-Trung and H. Wanner. 1992. Chemical Thermodynamics of Uranium, Elsevier, North Holland, Amsterdam. Griffiths, M., B.W. Gilbert and G.J.C. Carpenter. 1097. Phase instability, decomposition and redistribution of intermetallic precipitates in Zircaloy-2 and -4 during neutron irradiation. Journal of Nuclear Materials 150, 53-66.

Guillamont, R., R.T. Fanghanel, I. Grenthe, V. Neck, D. Palmer and M.H. Rand. 2003. Update on the chemical thermodynamics of uranium, neptunium, plutonium, americium and technetium.; In Chemical Thermodynamics, Elsevier, Amsterdam, Holland, 182-187.

Gwinner, B., F. Balbaud-Célérier, P. Fauvet, N. Gruet, P. Laghoutais, F. Miserque and R. Robin. 2022. A step towards a better understanding of corrosion of zirconium in nitric acid with additions of fluorine: Focus on the role of the presence of an initial oxide film. Corrosion Science 201, 110204.

Hall, D.S., M. Behazin, W.J. Binns and P.G. Keech. 2021. An evaluation of corrosion processes affecting copper-coated nuclear waste containers in a deep geological repository. Progress in Materials Science. 118, 100766.

Harada, M, and R. Wakamatsu. 2008. The effect of hydrogen on the transition behaviour of the corrosion rate of zirconium alloys. Zirconium in the Nuclear Industry; 15th International Symposium ASTM STP 1505, 384-400.

Hatano, Y., K. Isobe, R. Hitaka and M. Sugisaki. 1996. Role of intermetallic precipitates in hydrogen uptake of Zircaloy-2. Journal Nuclear Technology. 33, 944-949.

Heckmann, K. and J.Edward. 2020. Radionuclide inventory for reference CANDU fuel bundles. Nuclear Waste Management Organization Report NWMO-TR-2020-05, Toronto, Canada.

Hillner, E. 1964. Hydrogen absorption in Zircaloy during aqueous corrosion: Effect of Environment. U.S. Report WAPD-TM-411; Bettis Atomic Power Laboratory, W.Mifflin, PA, USA.

Hillner, E., D.G. Franklin and J.D. Smee. 1998. The corrosion of Zircaloy-clad assemblies in a geological repository environment. Report WAPD-T-3173; Bettis Atomic Power Laboratory, W.Mifflin, PA, USA.

Hillner, E., D.G. Franklin and J.D. Smee. 2000. Long-term corrosion of Zircaloy before and after irradiation. Journal Nuclear Materials 278, 334-345.

Hong, J-D., M. Park, A-M. Alvarez Holston and J. Stjärnsäter. 2021. Threshold stress intensity factor of delayed hydride cracking in irradiated Zircaloy-4 cladding. Journal of Nuclear Materials 543, 152596.

Hornkjoel. 1988. Pitting corrosion of zirconium and hafnium. Electrochimica Acta, 33, 289-292.

Hua, F., K. Mon, P. Pasupathi, G.M. Gordon and D.W. Shoesmith. 2004. Corrosion of Grade=7 and other Ti alloys in nuclear waste repository environments – A review. Corrosion 2004., Paper No. 04689, National Association of Corrosion Engineers, Houston, Texas.

Hua, F., K. Mon, P. Pasupathi, G. Gordon and D.W. Shoesmith. 2005. A review of corrosion of titanium grade-7 and other titanium alloys in nuclear waste repository environments. Corrosion 61, 987-1003.

Hummel, W., U. Berner, E. Curti, F.J. Pearson and T. Thoenen. 2002. Nagra/PSI chemical thermodynamic data base 01/01. Nagra Technical Report 02-16,. Wettingen, Switzerland.

Huot, J.Y. 1992. Electrochemical behaviour of zirconium metal and its oxide film in LiOH and HF solutions. Journal Applied Electrochemistry, 22, 852-858.

Hurlen, T. and S. Hornkjøl. 1991. Anodic growth of passive films on titanium. Electrochimica Acta 36, 189-195.

Hutchinson, B., B. Lehtinen, M. Limbaäck and M. Dahlbäck. 2007. A study of the structure and chemistry of Zircaloy-2 and the resulting oxide after high temperature corrosion. J.ASTM International (JAI), 4(10) (www.astm.org).

Ikeda, B., M.G. Bailey, C.F. Clarke and D.W. Shoesmith. 1990. Crevice corrosion and hydrogen embrittlement of titanium Grades-2 and -12 under Canadian waste vault conditions, Atomic Energy of Canada Limited, Report AECL-10121, Chalk River, Canada.

International Atomic Energy Agency (IAEA). 1998. Waterside corrosion of zirconium alloys in nuclear power plants. IAEA-TECDOC-996. Vienna, Austria.

International Atomic Energy Agency (IAEA). 2005. Assessment and management of ageing of major nuclear power plant components important to safety: BWR pressure vessel internals. IAEA-TECDOC-1471. Vienna, Austria.

International Atomic Energy Agency (IAEA). 2006. Understanding and managing aging of material in spent fuel storage facilities, IAEA Technical Reports Series No. 443, 26.

International Atomic Energy Agency (IAEA). 2015. Evaluation of conditions for hydrogen induced degradation of zirconium alloys during fuel operation and storage. Final Report of a Coordinated Research project (2011-2015). IAEA-TECDOC-1771. Vienna, Austria.

International Atomic Energy Agency (IAEA). 2015. Spent fuel performance assessment and research: Final report of a coordinated research project on spent fuel performance assessment and research (SPAR-III), 209-2014, IAEA-TECDOC-1771. Vienna, Austria.

International Atomic Energy Agency (IAEA). 2019. Behaviour of spent power reactor fuel during storage: Extracts from the final reports of coordinated research projects on behaviour of spent fuel assemblies in storage (BEFAST I-III) and spent fuel performance assessment and research (SPAR I-III); 1981-2014. IAEA-TECDOC-1862. Vienna, Austria.

International Atomic Energy Agency (IAEA). 2021. Spent fuel performance assessment and research: Final report of a coordinated research project (SPAR-IV). IAEA-TECDOC-1975, Vienna, Austria.

Jangg, G., R.T. Webster and M. Simon. 1978. Investigation into corrosion behaviour of zirconium alloys. IV. Pitting behavior of zirconium alloys. Werkstoffe und Korrosion. 29, 16-26.

Jensen, H. 2002. Properties of anodic oxide films on zirconium alloys. Ph.D. Thesis. The University of Western Ontario, London, Ontario, Canada.

Johnson, L.H. and P.A. Smith. 2000. The interaction of radiolysis products and canister corrosion products and the implications for spent fuel dissolution and radionuclide transport in a repository for spent fuel. Nagra Technical Report 00-04. Wettingen, Switzerland.

Johnson, L.H. and D.F. McGuinnes. 2002. Partitioning of radionuclides in Swiss power reactor fuels, Nagra Technical Report 02-07, Wettingen, Switzerland.

Johnson, L.H., J.C. Tait, D.W. Shoesmith, J.L. Crosthwaite and M.N. Gray. 1994. The disposal of Canada's nuclear fuel waste; Engineered barriers alternatives. Atomic Energy of Canada Limited Report, AECL-10718, COG-93-8. Chalk River, Canada.

Jones, C.F., R.L. Segall, R,St.C. Smart and P.S. Turner. 1977. Semiconducting oxides: the effect of prior annealing temperature on the dissolution kinetics of NiO. Journal Chemical Society: Faraday Transactions 1, 73, 1710-1720.

Kammerzind, B.F., D.G. Franklin, H.R. Peters and W.J. Duffin. 1996. Hydrogen pickup and redistribution in alpha-annealed Zircaloy-4: In Zirconium in the Nuclear Industry; 11th International Symposium ASTM STP 1295, 338-370.

Kato, O., H.Tanabe, T. Sakuragi, T. Nishimura and T. Tateishi. 2013. Corrosion tests of Zircaloy hull waste to confirm applicability of corrosion model and to evaluate influence factors on corrosion rates under geological disposal conditions. Materials Research Society Online Proceedings Library 1665, 195-202.

Kearns, J.J. 1967. Terminal solubility and partitioning of H in alpha zirconium, Zircaloy-2 and Zircaloy-4. Journal Nuclear Materials. 22, 304-310.

Keech, P.G., P. Vo, S. Ramamurthy, J. Chen, R. Jacklin and D.W.Shoesmith. 2014. Design and development of copper coatings for long-term storage of used nuclear fuel. Corrosion Engineering, Science and Technology. 49, 425-430.

Kim, Y.J. and R.A. Oriani. 1987a. Corrosion properties of the oxide film formed on Grade-12 titanium in brine under gamma radiation. Corrosion, 43, 85-91.

Kim, Y.J. and R.A. Oriani. 1987b. Brine radiolysis and its effect on the corrosion of Grade-12 titanium. Corrosion, 43, 92-97.

King, F. and S. Stroes-Gascoyne. 2000. An assessment of the long-term corrosion behaviour of C-steel and the impact of redox conditions inside a nuclear fuel waste disposal container. Ontario Power Generation Report No. 06819-REP-01200-10028-R00.

King, F., D.S. Hall and P.G. Keech. 2017. Nature of the near field environment in a deep geological repository and the implications for the corrosion behaviour of the container. Corrosion Engineering, Science and Technology. 52 (Sup 1) 25-30.

Kobayashi, T., T. Sasaki, I. Takagi and H. Moriyama. 2007. Solubility of zirconium (IV) hydrous oxides. Journal Nuclear Science and Technology. 44, 90-94.

Kobayashi, T., D. Bach, M. Altmaier, T. Sasaki and H. Moriyama. 2013. Effect of temperature on the solubility and solid phase stability of zirconium hydroxide. Radiochimica Acta. 101, 645-651.

Kong, D-S. 2008. The influence of fluoride on the physicochemical properties of anodic oxide films formed on titanium surfaces. Langmuir 24, 5324-5331.

Knittel, D.R., M. A. Maguire, A. Bronson and J-S. Chen. 1982. The effect of surface treatments and electrochemical methods on the pitting potential of zirconium in chloride solutions. Corrosion, 38, 265- 273.

Knittel, D.R. and A. Bronson. 1984. Pitting corrosion on zirconium – A review. Corrosion, 40, 9-14.

Kurashige, T., R. Fujisawa, Y. Inagaki and M. Senoo. 1999. Gas generation behavior of Zircaloy-4 under waste disposal conditions. Radioactive Waste Management and Environmental Remediation. ICEM Conference Proceedings, ASME, Nagoya, Japan, September 1999.

Lampman, T.J. and T.A. Daniels. 2005. Proposed tests and examinations to provide assurance of fuel integrity during dry storage and subsequent handling. Ontario Power Generation Report 06819-REP-03720-00009-R00. Toronto, Canada.

Lampman, T.J. and A. Popescu. 2008. CANDU fuel bundle stress model for used fuel dry storage analysis. AMEC NSS Document NW007/RP/001 R00. Toronto, Canada.

Lampman, T.J. and P. Gillespie. 2010. Assessment of delayed hydride cracking in used CANDU fuel bundles during dry storage. Nuclear Waste Management Organization Report NWMO-TR-2010-13. Toronto, Canada.

Lampman, T.J. and A. Popescu. 2010. Initial evaluation of mechanical stress distributions in spent CANDU fuel bundles. Nuclear Waste Management Organization Report NWMO TR-2010-11. Toronto, Canada.

Landolt, D., A. Davenport, J. Payer and D.W. Shoesmith. 2008. A review of materials and corrosion issues regarding canisters for disposal of spent fuel and high-level waste in Opalinus clay, Nagra Technical Report NTB-09-02, Wettingen, Switzerland.

Lavigne, O., T. Shoji and K. Sakaguchi. 2012. On the corrosion behaviour of Zircaloy-4 in spent fuel pools under accident conditions. Journal of Nuclear Materials 426, 120-125.

Leach, J.S.L. and B.R. Pearson. 1988. Crystallization in anodic oxide films. Corrosion Science. 28, 43-56. Lefebvre, F. and C. Lemaignan. 1997. Irradiation effects on corrosion of zirconium alloy cladding. Journal of Nuclear Materials 248, 268-274.

Lee, C.T., Z. Qin, M. Odziemkowski and D.W. Shoesmith. 2006. The influence of groundwater anions on the impedance behaviour of carbon steel corroding under anoxic conditions. Electrochimica Acta, 51, 1558-1568.

Leitner, K., J.W. Schultze and U. Stimming. 1986. Photoelectrochemical investigations of passive films on titanium electrodes. Journal Electrochemical Society. 133, 1561-1568.

Li, X., F. Gui, H. Cong, C.S. Brossia and G.S. Frankel. 2013. Examination of mechanisms for liquid-air-interface corrosion of steel in high-level radioactive waste simulants. Journal Electrochemical Society 160, C521-C530.

Little, B.J., P.A. Wagner and R.I. Ray. 1992. An experimental evaluation of titanium's resistance to microbiologically influenced corrosion. Corrosion 92, National Association of Corrosion Engineers, Houston, TX, Paper No. 173.

Little, B.J., P.A. Wagner and R.I. Ray. 1993. An evaluation of titanium exposed to thermophilic and marine biofilms. Corrosion 93, National Association of Corrosion Engineers, Houston, TX, USA, Paper No. 308.

Lorenzo de Melo, M.F., M.C. Cortizo. 2000. Electrochemical behaviour of titanium in fluoride-containing saliva. Journal Applied Electrochemistry. 30, 95-100.

Lovasic, Z. and J.E. Villagran. 2004. Used fuel integrity during dry storage: investigation program. Ontario Power Generation Report 06819-REP-03729-00006. Toronto, Canada.

Lovasic, Z. and P. Gierszewski. 2005. CANDU fuel long-term storage and used fuel integrity. Proc. 9th Canadian Nuclear Society International Conference on CANDU fuel. Canadian Nuclear Society, Toronto, Canada.

Lowalekar, V. and S. Raghavan. 2004. Etching of zirconium oxide, hafnium oxide, and hafnium silicates in dilute hydrofluoric acid solutions. Journal Materials Research. 19, 1149-1156.

Macdonald, D.D. 1999. Passivity – the key to our metals-based civilization. Pure and Applied Chem., 71, 951-978.

Magoda, A.S. 1999a. Electrochemical behaviour of zirconium and the anodic oxide film in aqueous solutions containing chloride ions. Thin Solid Films 357, 202-207.

Magoda, A.S. 1999b. Influence of some parameters on passivation of zirconium and the stability of the anodic oxide film. Corrosion 55, 877-882.

Maguire, M. 1984. The pitting susceptibility of zirconium in aqueous Cl^-, Br^- and I^- solutions. Industrial Applications of Titanium and Zirconium: Third Conference, ASTM STP 830, R.T. Webster and C.S. Young, Eds. American. Society for Testing and Materials, *pp.* 175-*189.*

Mamun, A., R. Schennach, J.R. Parga, M.Y.A. Mollah, M.A. Hossain and D.L. Cocke. 2001. Passive film breakdown during anodic oxidation of zirconium in pH 8 buffer containing chloride and sulfate. Electrochimica Acta, 46, 3343-3350.

Mankowski, G., Y. Roques and F. Dabosi. 1989. Effect of passive film growth on the kinetics of pit generation on Zircaloy-4. Materials Science Forum, 44-45, 279-288.

Mansfeld, F. and B.J. Little. 1991. A technical review of electrochemical techniques applied to microbiologically influenced corrosion. Corrosion Science 32, 247-272.

Mansfeld, F., R. Tsai, H. Shih, B.J. Little, R. Ray and P. Wagner. 1990. Results of exposure of stainless steels and titanium to natural seawater. Corrosion 90, National Association of Corrosion Engineers, Houston, TX, USA, Paper No.109.

Mansfeld, F., R. Tsai, H. Shih, B.J. Little, R. Ray and P. Wagner. 1992. An electrochemical and surface analytical study of stainless steels and titanium exposed to natural seawater. Corrosion Science 33, 445-456.

Mansfeld, F., G. Liu, H. Xiao, C.H. Tsai and B.J. Little. 1994. The corrosion behaviour of copper alloys, stainless steels and titanium in seawater, Corrosion Science 36, 2063-2095.

Mardon, J.P. 2008. Matériaux des tubes de gainage pour réacteurs à eau pressurisée, techniques de l'ingénieux, Traite Génie nucléaire, Article BN 3700, Juillet.

Marici, D., G. Bolat, A. Cailean, J.J. Santana, J. Izquierde and R.M. Souto. 2014. Effect of acidic fluoride solution on the corrosion resistance of ZrTi alloys for dental implant application. Corrosion Science. 87, 334-343.

Mandry, M.J. and Rosenblatt, G. 1972. Investigating products of titanium dissolution in the presence of fluoride ions with dual dynamic voltammetry. Journal Electrochemical Society. 119, 29-33.

McMinn, A., E.C. Darby and J.S. Schofield. 2000. The terminal solid solubility of hydrogen in zirconium alloys. In Zirconium in the Nuclear Industry: 12th International Symposium ASTM STP 1354, 173-195.

Meisterjahn, P., H.W. Hoppe and J.W. Schultze. 1987. Electrochemical and XPS measurements on thin oxide films on zirconium. Journal of Electroanalytical Chemistry, 217, 159-185.

Millero, F.J. and S. Sotolongo. 1989. The oxidation of Fe(II) with H_2O_2 in seawater. Geochimica Cosmochimica Acta. 53, 1867-1873.

Morco, R.P., J.M. Joseph, D.S. Hall, C. Medri, D.W. Shoesmith and J.C. Wren. 2017. Modelling of radiolytic production of HNO_3 relevant to corrosion of a used fuel container in deep geologic repository environments. Corrosion Engineering, Science and technology 52 (sup 1), 141-147.

Motta, A.T. and L.-Q. Chen. 2012. Hydride formation in zirconium alloys. Journal Metals 64, 1403-1408.

Motta, A.T., A.Couet and R.J. Comstock. 2015. Corrosion of zirconium alloys used for nuclear fuel cladding. Annual Review of Materials Research 45, 311-343.

Necib, S., C. Bueur, S. Caes, F. Cochin, B.Z. Cvetković, M. Fulger, J.M. Gras, M. Hern, L. Kasprzak, S. Legand, V. Metz, S. Perrin, T. Skuragi and T. Suzucki-Muresan. 2018. Overview of ^{14}C release from irradiated Zircaloys in geological disposal conditions. Radiocarbon, 60, 1757-1771.

Ni, N., S. Lozano-Perez, M.L. Jenkins, C. English, G.D.W. Smith and J.M. Sykes. 2010. Porosity in oxides on zirconium fuel cladding alloys and its importance in controlling oxidation rates. Scripta Materialia. 62, 564-567.

Noël, J., H.L. Jensen, Z. Tun and D.W. Shoesmith. 2000. Electrochemical modification of the passive oxide layer on Zr-2.5Nb observed by in-situ neutron reflectometry. Electrochemical and Solid State Letters. 3, 473-476.

Noël, J.J., D.W. Shoesmith and B.M. Ikeda. 2001. Crevice corrosion of alpha titanium alloys. In: Proceedings of the Research Topical Symposia, NACE Corrosion/2001, Houston, Texas, March 11-16, 2001 (G,S. Frankel and J.R. Scully, Eds), NACE International, Houston, Texas, USA, 65-102.

Noël, J., D.W. Shoesmith and Z. Tun. 2008. Anodic oxide growth and hydrogen absorption on Zr in neutral aqueous solution: A comparison to Ti. Journal Electrochemical Society. 155, C444-C454.

Nuclear Waste Management Organization (NWMO). 2017. Postclosure safety assessment of a used fuel repository in crystalline rock. Nuclear Waste Management Organization Report NWMO-TR-2017-02.

Nuclear Waste Management Organization (NWMO). 2018. Post closure safety assessment of a used fuel repository in sedimentary rock. Nuclear Waste Management Organization Report NWMO-TR-2018-08.

Ortega, C. and J. Siejka. 1982. A study by nuclear microanalysis and ^{18}O tracing of the growth of anodic oxide films on zirconium. Journal of Electrochemical Society, 129, 1905-1917.

Pan, J., D. Thierry and C. Leygraf. 1994. Electrochemical and XPS studies of titanium for biomaterial applications with respect to the effect of hydrogen peroxide. Journal of Biomedical Materials Research, Part A, 28, 113-122.

Pan, J., D. Thierry and C. Leygraf. 1996. Hydrogen peroxide toward enhanced oxide growth on titanium in PBS solution: Blue coloration and clinical relevance. Journal of Biomedical Materials Research Part A, 30, 393-402.

Pan, J., C. Leygraf, D. Thierry and A.M. Ektessabi. 1997. Corrosion resistance for biomaterial applications of TiO_2 films deposited on titanium and stainless steel by ion-beam-assisted sputtering. Journal Biomedical Materials Research 35, 309-318.

Pan, Y.M., C.S. Brossia, G.A. Cragnolino, V. Jain, O. Pensado and N. Sridhar. 2001. Effect of in-package chemistry on the degradation of vitrified high-level radioactive waste and spent nuclear fuel cladding. Center for Nuclear Waste Regulatory Analyses, Report CNWRA 2002-01, 37-52, San Antonia, TZ, USA.

Pastina, B., J. Isabey and B. Hickel. 1999. The influence of water chemistry on the radiolysis of primary coolant water in pressurized water reactors. Journal Nuclear Materials 264, 309-318.

Pastina, B. and J.A. LaVerne. 2001. Effect of molecular hydrogen on hydrogen peroxide in water radiolysis. Journal Physical Chemistry A 105, 9316-9322.

Pease, W.R., R.L. Segall, R.St.C. Smart and P.S. Turner. 1986. Comparative dissolution rates of defective nickel oxides from different sources. Journal Chemical Society Faraday Transactions 1, 82, 759-766.

Pecheur, D., F. Lefebvre, A.T. Motta, C. Lemaignan and C. Wadier. 1992. Precipitate evolution in the Zircaloy-4 oxide layer. Journal Nuclear Materials. 189, 2318-2332.

Pecheur, D., F. Lefebvre, A.T. Motta, C. Lemaignan and C. Charquet. 1994. Oxidation of intermetallic precipitates in Zircaloy-4: Impact of irradiation; In 10th International Symposium on Zirconium in the Nuclear Industry, ASTM STP-1245, 687-705.

Pinard-Legry, G., M.Pelras and G. Turluer. 1989. Corrosion resistance of metallic materials in nuclear fuel reprocessing – A Working Party Report on Corrosion in the Nuclear Industry, EFC publications, The Institute of Metals, 1, 47-51.

Platt, P., E. Polatidis, P. Frankel, M. Klaus, M. Gass, R. Howells and M. Preuss. 2015. A study into stress relaxation in oxides formed on zirconium alloys. Journal Nuclear Materials 456, 415-425.

Popescu, A. and T. Lampman. 2010. CANDU fuel element model development and sensitivity study. Nuclear Waste Management Organization Report NWMO TR-2010-12. Toronto, Canada.

Porte, H.A., J.G. Schnizlein, R.C. Vogel and D.F. Fisher. 1960. Oxidation of zirconium and zirconium alloys. Journal Electrochemical Society 107, 506-515.

Pourbaix, M. 1970. Significance of protective potential in pitting and intergranular corrosion. Corrosion 26, 431-438.

Qui, L., D.A. Guzonas and D.G. Webb. 2009. Zirconium solubility in high temperature aqueous solution. J.Soln.Chem. 38, 857-867

Rämö, K. Saarinen and M. Sillanpää. 2002. Uniform corrosion of titanium in alkaline hydrogen peroxide conditions: Influence of transition metals and inhibitors calcium and silicate. Materials and Corrosion 53, 898-901.

Reilly, T. 2022. Nuclear fuel waste projections in Canada – 2022 update. Nuclear Waste Management Organization NWMO-TR-2022-17.

Rodriguez, C., D.A. Barbiric, M.E. Pepe and J.A. Kovacs. 2002. Metastable phase stability in the ternary Zr-Fe-Cr system. Intermetallics 10, 205-216.

Rothman, A.J. 1984. Potential corrosion and degradation mechanisms of Zircaloy cladding on spent nuclear fuel in a tuff repository. Lawrence Livermore National Laboratory Technical Report UCID 20172, Livermore, CA, USA.

Sakuragi, T., H. Miyakawa, T. Nishimura and T. Tateishi. 2012. Corrosion rates of Zircaloy-4 by hydrogen measurement under high pH, low oxygen and low temperature conditions. Materials Research Society Online Proceedings Library, 1475, 311-316.

Satpati, A.K., S.V. Phadnis and R.I. Sundaresan. 2005. Electrochemical and XPS studies and the potential scan rate dependent pitting corrosion behaviour of Zircaloy-2 in 5% NaCl solution. Corrosion Science, 47, 1445-1458.

Segall, R.L., R.St,C, Smart and P.S. Turner. 1988. Oxide surfaces in solution, In: Surface and Near Surface Chemistry of Oxide Materials, edited by J. Nowotny and L.-C. Dufour, Elsevier Science Publishers, Amsterdam, Chapter 13, 5270576.

Shaltiel, D., I. Jacob and D. Davidov. 1977. Hydrogen absorption and desorption properties of AB_2 Laves-phase pseudobinary compounds. Journal Less Common Metals, 53, 117-131.

Sherar, B.W.A., P.G. Keech, J.J. Noël, R.G. Worthington and D.W. Shoesmith. 2013. Effect of sulphide on carbon steel corrosion in anaerobic near-neutral pH saline solutions. Corrosion, 69, 67-76.

Shek, G.K. and B.S. Wasiluk. 2009. Development of delayed hydride cracking test apparatus and commissioning tests for CANDU fuel bundle assembly welds. Nuclear Waste Management Organization Report NWMO-TR-2009-08, Toronto, Canada.

Shek, G.K. 2010. Determination of the threshold stress intensity factor and velocity of delayed hydride cracking of endplate welds in CANDU fuel bundles with different design and manufacturers. Nuclear Waste Management Organization Report NWMO-TR-2010-25, Toronto, Canada.

Shibata, T. and Y.-C Zhu. 1995. The effect of film formation conditions on the structure and composition of anodic oxide films on titanium. Corrosion Science, 37, 253-270.

Shoesmith, D.W. and F. King. 1999. The effects of gamma radiation on the corrosion of candidate materials for the fabrication of nuclear waste packages. Atomic Energy of Canada Limited Report AECL-11999, Chalk River, Canada.

Shoesmith, D.W. 2006. Assessing the corrosion performance of high-level nuclear waste containers. Corrosion. 62, 703-722.

Shoesmith, D.W. and B.M. Ikeda. 1997. The resistance of titanium to pitting, microbially induced corrosion, and corrosion under unsaturated conditions. Atomic Energy of Canada Limited Report AECL-11709, COG-96-557-1. Chalk River, Canada.

Shoesmith, D.W. and D. Zagidulin. 2011. The corrosion of zirconium under deep geological repository conditions. Journal of Nuclear Materials, 418, 292-306.

Smailos, E., W. Schwarzkopf and R. Koster. 1986. Corrosion behaviour of container materials for disposal of high-level wastes in rock salt environments, Nuclear Science and Engineering, Commission of the European Communities, Luxembourg, EUR-10400-EN.

Smailos, E. and R. Koster. 1987. Corrosion studies on selected packaging materials for disposal of high level wastes; In “Materials Reliability in the Back End of the Nuclear Fuel Cycle. International Atomic Energy Agency TECDOC-421, 7-24. IAEA, Vienna, Austria.

Smart, N.R., D.J. Blackwood and L. Werme. 2002a. Anaerobic corrosion of carbon steel and cast iron in artificial groundwaters: Part 1 – Electrochemical aspects, Corrosion, 58, 547-559.

Smart, N.R., D.J. Blackwood and L. Werme. 2002b. Anaerobic corrosion of carbon steel and cast iron in artificial groundwaters: Part 2 – Gas generation; Corrosion, 58, 627-637.

Sutton, H.C. and C.C. Winterbourn. 1989. On the participation of higher oxidation states of iron and copper in Fenton reactions. Free Radical Biology and Medicine. 6, 53-60.

SKB 1999. SR97 Processes in the repository evolution. Swedish Nuclear Fuel and Waste Management Company Technical Report, TR-99-07, Solna, Sweden.

SKB. 2006. Fuel and canister progress report for the safety assessment SR-Can. Swedish Nuclear Fuel and Waste Management Company, Solna, Sweden.

Tanabe, H., T. Sakuragi, H, Miyakawa and R. Takahashi. 2913. Long-term corrosion of Zircaloy hull waste under geological disposal conditions: Corrosion correlations, factors influencing corrosion, corrosion test data and preliminary evaluation. Scientific Basis for Nuclear Waste Management XXXVII, Barcelona, Spain. September 29 – October 3, 2013 Mat.Res.Soc.Symp.Proc 1518

Tengvall, P., H. Elwing, L. Sjöqvist and L.M. Djursten. 1989a. Interaction between hydrogen peroxide and titanium: a possible role in the biocompatibility of titanium. Biomaterials 10, 118-120.

Tengvall, P., I. Lundström, L. Sjöqvist, H. Elwing and L.M. Bjursten. 1989b. Titanium-hydrogen peroxide interaction: model studies of the influence of the inflammatory response on titanium implants. Biomaterials, 10, 166-175.

Tupin, M., M. Pijolit, F. Valdivieso, M. Soustelle, A. Frichet and P. Barbaris. 2003. Differences in reactivity of oxide growth during the oxidation of Zircaloy-4 in water vapour before and after the kinetic transition. Journal Nuclear Materials 317, 130-144.

Turnbull, J.R., R. Szukalo, M. Behazin, D. Hall, D. Zagidulin, S. Ramamurthy, J.C. Wren and D.W. Shoesmith. 2018. The effects of cathodic reagent concentration and small solution volumes on the corrosion of copper in dilute nitric acid solutions. Corrosion 74, 326-336.

Une, K. and S. Ishimoto. 2003. Dissolution and precipitation behaviour of hydrides in Zircaloy-2 and high Fe Zircaloy. Journal Nuclear Materials 332, 66-72.

Une, K., K. Sakamoto, M. Aomi, J. Matsunaga and Y. Etoh. 2011. Hydrogen absorption mechanism of zirconium alloys based on characterization of the oxide layer. Zirconium in the Nuclear Industry, 16th International Symposium, ASTM STP 1529, 401-432.

Verlet, R. 2015. Influence of irradiation and radiolysis on the corrosion rates and mechanisms of zirconium alloys. Ecole Nationale Superieure des Mines de Saint-Etienne, Saint Etienne, France (In French).

Vo, P., D. Poirier, J.-G. Legoux, P.G. Keech, D. Doyle, P. Jakupi and E. Irisson. 2015. Development of cold spray technology for copper coating of carbon steel used fuel container prototypes for CANDU fuel. Nuclear Waste Management Organization Report NWMO-TR-2015-29, Toronto, Canada.

Wada, R.T., T. Nishimura, K. Fujiwara, M. Tanabe and M. Mihara. 1999. Experimental study on hydrogen gas generation rate from corrosion of Zircaloy and stainless steel under anaerobic alkaline conditions. Seventh International Conference on Radioactive Waste Management and Environmental Remediation. ICEM Conference Proceedings, ASME, Nagoya, Japan, 26-30 September.

Wei, J., P. Frankel, E. Polatidis, M. Blat, A. Ambard and R.J. Comstock. 2013. The effect of Sn on autoclave corrosion performance and corrosion mechanisms in Zr-Sn-Nb alloys. Acta Materialia, 61, 4200-4214.

Wilhelmsen, W. and A.P. Grande. 1987. The influence of hydrofluoric acid and fluoride on the corrosion and passive behaviour of titanium. Electrochimica Acta, 32, 1469-1474.

Xu, W., K. Daub, X. Zhnag, J.J. Noël, D.W. Shoesmith and J.C. Wren. 2009. Oxide formation and conversion on carbon steel in mildly basic solutions. Electrochimica Acta, 54, 5727-5738.

Yang, Q,, E. Toijer and P. Olsson. 2019. Analysis of radiation damage in the KBS-3 canister materials. Swedish Nuclear Fuel and Waste Management Company Technical Report TR-19-14, Solna, Sweden.

Yau, T-L. 2005. Corrosion of zirconium and zirconium alloys. ASM handbook Vol. 13B: Materials edited by S.D. Cramer and B.S. Covino Jr. 300-324. ASM International, Materials Park, OH, USA.

Yau, T.-L. and R.C. Sutherlin. 2005. Corrosion of zirconium and zirconium alloys. 2005. ASM Handbook, Volume 13B: Corrosion; Materials; edited by S.D. Cramer and B.S, Covibo Jr., 300-324. ASM International, Materials Park, OH, USA.

Yilmazbayhan, A., E. Breval, A.T. Motta and R.J. Comstock. 2006. Transmission electron microscopy examination of oxide layers formed on Zr alloys. Journal of Nuclear Materials, 349, 265-281.

Zeng, Y. 2009. Passive film properties and their influence on hydrogen absorption into titanium. Ph.D. Thesis, University of Western Ontario, London, Canada.

Zepp, R.G., B.G. Faust and J. Hoigné. 1992. Hydroxyl radical formation in aqueous reactions (pH 3-8) of iron (II) with hydrogen peroxide. The photo-Fenton reaction. Environmental Science and Technology, 26, 313-319.

Zhang, Y. 2017. Corrosion of titanium, zirconium and their alloys for biomedical applications. Ph.D. Thesis. University of Birmingham, Birmingham, UK.

Zumpicchiatt, G., S. Pascal, M. Tupin and C. Berdin-Meric. 2015. Finite element modelling of the oxidation kinetics of Zirvcaloy-4 with a controlled metal oxide interface and the influence of growth stress. Corr.Sci. 100, 209-221.

APPENDIX A

A.1 THE PROPERTIES OF THE OXIDE FILMS ON TITANIUM AND ZIRCONIUM

Both Ti and Zr alloys are commonly used in industrial applications where corrosion resistance to aggressive environments is required (Schutz and Thomas 1987, Been and Grauman 2000, Shoesmith and Noël 2010). Both bare metals spontaneously oxidize to produce a thin, chemically inert, oxide film which renders the metal passive and unreactive. While both passivated metals (and alloys) are very stable, the properties of their protective oxides are different and this confers some differences in corrosion properties on the two materials. The oxide film on Ti is a semiconductor with a wide band gap of 3.05 eV and slight deviations from stoichiometry (TiO_{2-x}) give the oxide film n-type characteristics (Torresi et al. 1987). These n--type characteristics can be attributed to a combination of O_V and interstitial Ti^{III} ions which lead to the trapping of electrons in a band orbital just below the conduction band edge (Jarzebski 1973, Shoesmith and Ikeda 1997). By contrast, ZrO_2 is an insulator with a very large band gap (>5 eV) (Meisterjahn et al. 1987).

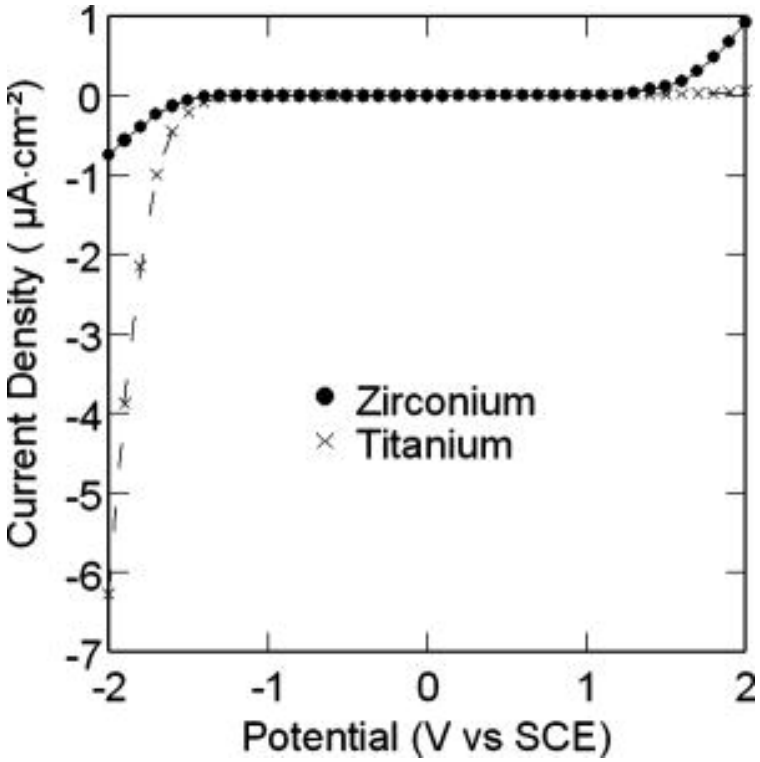

Figure 1A: Polarization behaviour of Ti and Zr in neutral 0.1 mol/L $KClO_4$ solution (Noël et al. 2008).

Electrochemically-determined polarization curves (Noël et al. 2008), Figure 1A, show that both metals display a wide passive potential region within which they are electrochemically inert and, hence, corrosion resistant. However, when polarized to positive (anodic) or negative (cathodic) potentials, both materials exhibit significant loss of passivity. At positive potentials, Zr loses passivity more readily than Ti exhibiting substantial current for potentials ≥1.3 V (vs. the

Saturated Calomel Electrode (SCE)), while at more negative potentials, Ti more readily supports the cathodic reduction of H_2O at potentials ≤1.5 V (vs. SCE), Figure 1A.

For both metals, anodic polarization leads to oxide growth, but the nature of the growth process and the properties of the oxides are different. For both metals the anodization ratio (increase in oxide thickness per volt applied) is similar, a value of ~2.5 nm/V being obtained for Ti (Tun et al. 1999) compared to 2.8 nm/V (Meisterjahn et al. 1987) to 3.4 nm/V (Noël et al. 2008) for Zr. The differences in film growth behaviour can be explained by the differences in growth mechanism. Anodic films on Zr are crystalline (Cox 1970, Leach and Pearson 1988, Ortega and Siejka 1982), while those on Ti are initially amorphous and undergo potential-induced crystallization only at high potentials (Shibata and Zhu 1995).

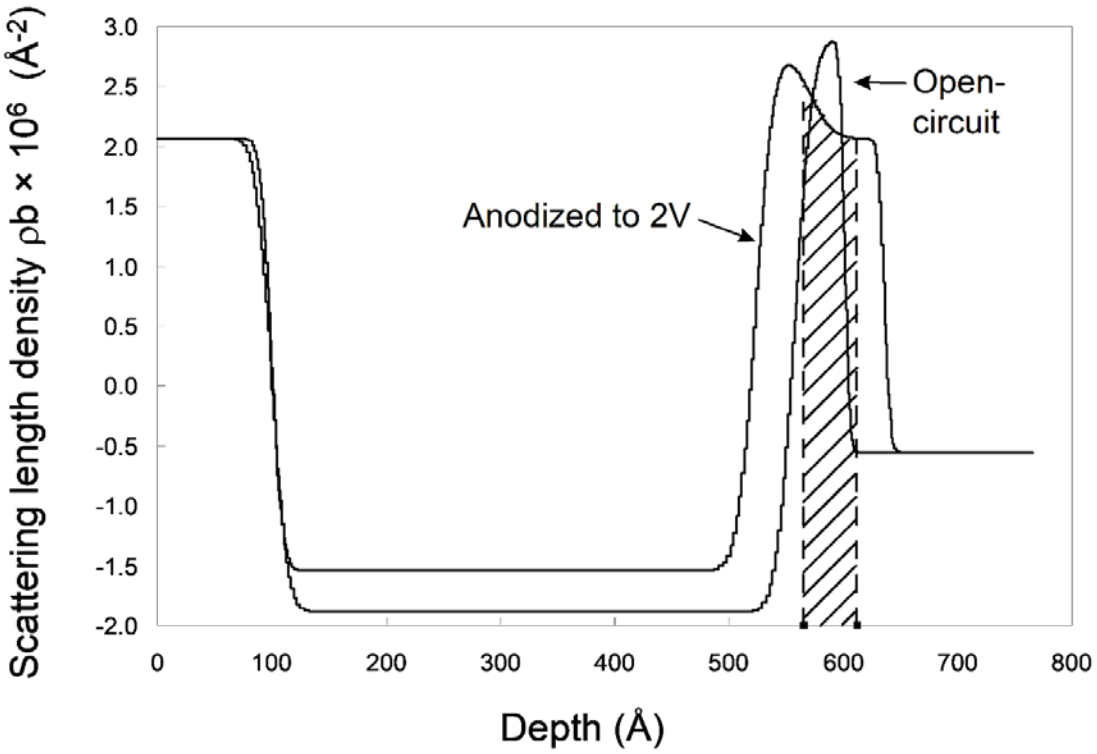

Figure 2A: Neutron reflectometry profiles (expressed as the scattering length density (SLD), an indicator of composition) showing the distinct layers comprising the electrode: 0 to ~100 Å, the Si wafer substrate; 100 to ~500 Å, the sputtered Ti layer; ~500 Å to ~650 Å, the air-formed oxide film (open circuit) and the film grown anodically at an applied potential of 2 V; ≥650 Å, the aqueous electrolyte solution (neutral 0.27 mol/L NaCl). The shaded region shows the expected position of the original air-formed oxide within the anodically grown film (Tun et al. 1999).

Oxidization of Zr is dominated by the migration of oxygen to the metal oxide interface leading to a stress build up at this interface as a consequence of the large Pilling-Bedworth (P-B) ratio of ~1.5 (Noël et al. 2000). (The P-B ratio is the ratio of the volume of oxide created to the volume of metal consumed). This leads to a stress-induced crystallization and the introduction of migration pathways most likely along crystalline grain boundaries (Cox 1970). For Ti, even though the Pilling-Bedworth ratio is even larger (1.72; Tun et al. 1999), stress-induced

crystallization does not occur. This can be attributed to the fact that both anion and cation transport occur during oxide growth, the transport numbers being 0.65 and 0.35, respectively (Khalil and Leach 1986). Growth under these conditions avoids stress build-up since the volume of the oxide grown at the metal/oxide interface is just sufficient to replace the volume of metal converted, the remaining oxide growth occurring at the oxide/solution interface where stress-free expansion is possible.

The consequences of these differences can be seen in in-situ neutron reflectometry experiments conducted with the metal subjected to an applied electrochemical potential. Anodic oxidation of Ti results in the formation of a dense rutile structure with H only present in the outer region of the film at the oxide/solution interface (Tun et al. 1999), Figure 2A. X-ray photoelectron spectroscopic analyses indicate the H is in the form of OH^- ions or H_2O. These results demonstrate that, for Ti, while incorporation of OH^-/H_2O occurs under oxidizing conditions, it is confined to a layer of $TiO_2 \bullet H_2O$ at the oxide/solution interface. At the metal/oxide interface a dense, protective layer of rutile, similar in properties to that formed by air exposure, persists.

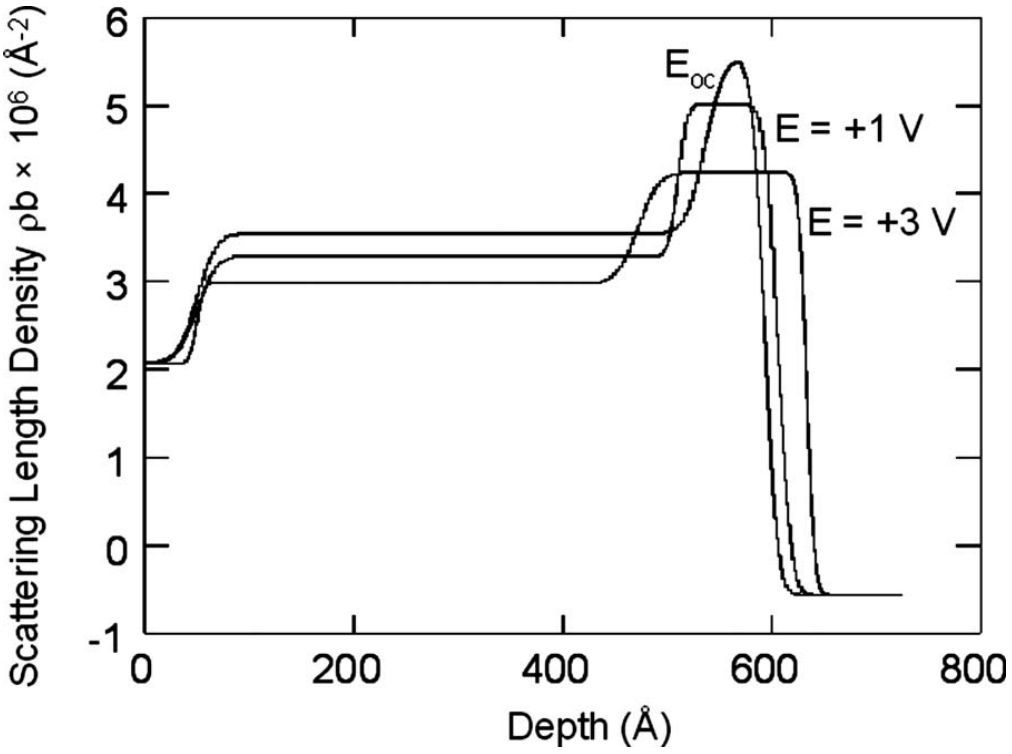

Figure 3A: Neutron reflectometry profiles recorded on a Zr electrode showing similar layers to those identified in Figure 2A for Ti. The profile for the air-formed film present on open-circuit is marked E_{OC}. The other two profiles were obtained after anodic oxidation at 1 V and 3 V (vs. SCE), respectively. The decrease in SLD in the oxide as the applied potential is increased indicates an increase in hydrogen content with increasing oxide growth. The constant SLD throughout the oxide indicates the presence of H throughout the film from the metal/oxide interface (at ~45 Å (3 V)) to the oxide/electrolyte solution interface (at ~650 Å (3 V)) (Noël et al. 2008).

By contrast, similar experiments on Zr, again initially covered by an air-formed oxide, show that under anodic oxidizing conditions, the film, while remaining intact and protective, incorporates OH^-/H_2O throughout the film including in the "dry" air-formed oxide initially present, Figure 3A (Noël et al. 2008). The decrease in neutron scattering length density (SLD) for the metal itself shows H is also absorbed into the metal despite the application of a positive applied potential.

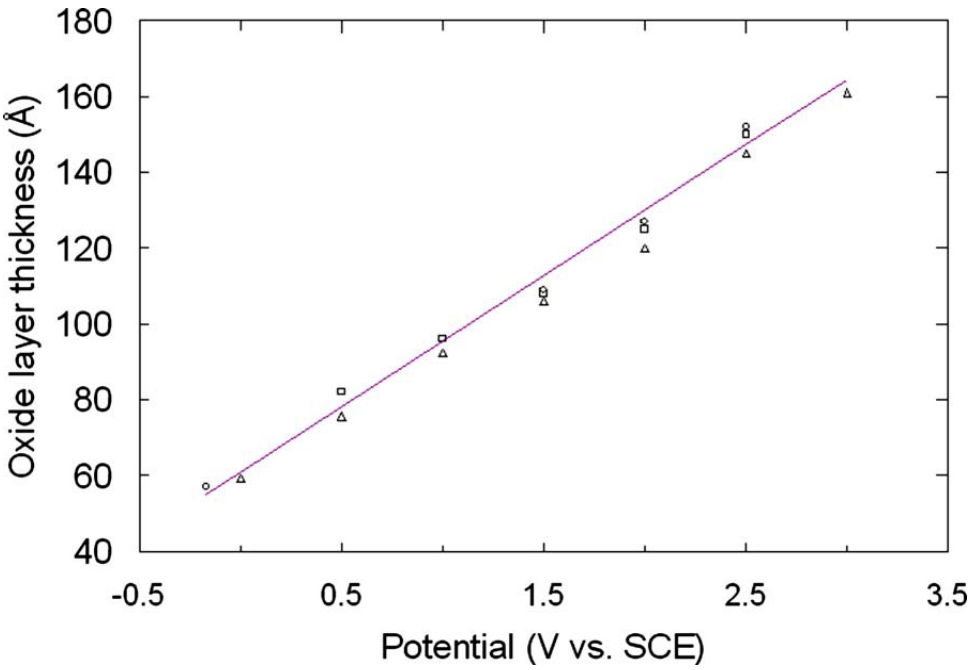

Figure 4A: Oxide layer thickness, determined in neutron reflectometry experiments, as a function of applied potential on Zr in a neutral 0.1 mol/L Na_2SO_4 solution. The symbols, Δ □ ○ show that, while a slight thickening of the oxide occurs with time (6, ~12, ~18 hours, respectively) the thickness has almost achieved a steady-state value (Noël et al. 2008)

Figures 4A and 5A show the increase in oxide thickness and decrease in SLD, respectively, as the oxidation potential is increased. The SLD is indicative of the composition and density of the film, and the decrease in SLD as the applied potential is made more positive indicates the incorporation of H, an atom with a negative SLD. These neutron experiments show that even a small change in oxidation potential changes the properties throughout the full depth of the oxide on Zr. Accompanying impedance measurements show that, despite the steady decrease in SLD indicating a potential-dependent increase in OH^-/H_2O content of the film as the potential is made more oxidizing, Figure 5A, there is no loss in protectiveness of the oxide due to the introduction of these H_2O-containing migration pathways until the potential reaches 1.5 V. When this potential is reached or exceeded, loss of protectiveness is clearly visible as a sudden further increase in OH^-/H_2O (decrease in SLD), Figure 5A. The decrease in SLD of the metal, Figure 3A, indicates that the potential at the base of grain boundaries/fractures in the oxide is decoupled from the applied potential, due to the high resistance (R) of the grain boundaries/fractures which leads to an ohmic (IR) drop in potential when an electrochemical current (I) is flowing. This allows H_2O reduction at the Zr/oxide interface resulting in H absorption into the Zr.

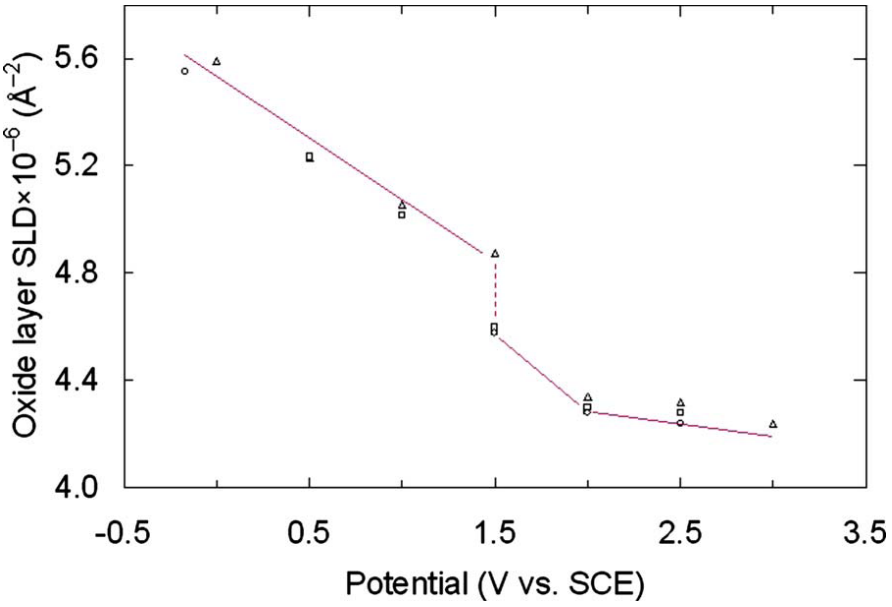

Figure 5A: The scattering length density (SLD) of the oxide film on Zr determined by neutron reflectometry after anodic oxidation at various applied potentials. The data points have the same significance as in Figure 4A. The decrease in SLD shows that the hydrogen content of the oxide increases steadily as the potential increases up to ~1.5 V, and then suddenly increases as the film undergoes fracture (Noël et al. 2008).

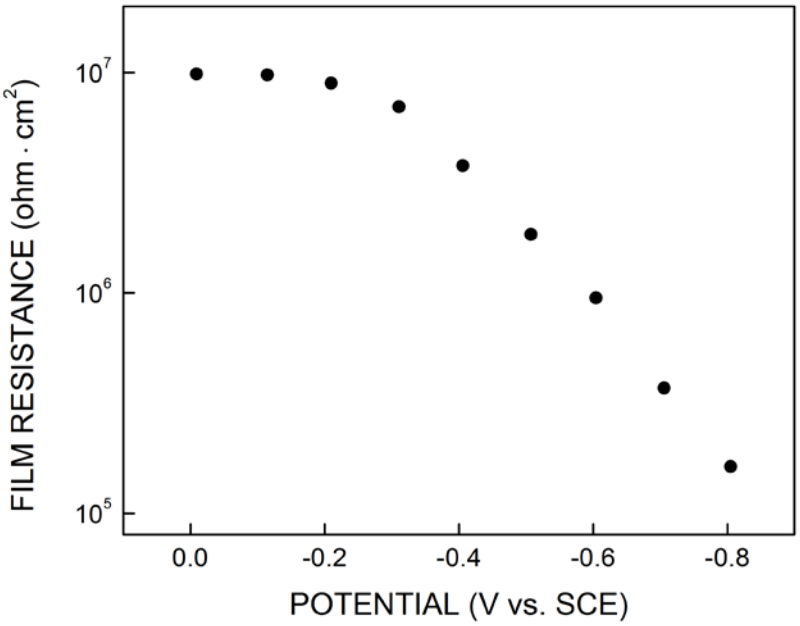

Figure 6A: Variation of the oxide film resistance on Grade-2 Ti as a function of applied potential in a deaerated neutral 0.27 mol/L NaCl solution. The resistance was determined by electrochemical impedance spectroscopy on an oxide pre-grown by anodic oxidation at 0.6 V (vs. SCE) for 48 hours (Zeng 2009).

These differences in film growth between the two materials are consistent with expectations based on the cation/anion transport numbers. Given the known crystalline nature of the ZrO_2 film, it can be concluded that Zr, but not Ti, contains pathways (crystalline grain boundaries, tight flaws and/or pores) along which water soluble species can migrate. As discussed in section 8, this difference can explain why Zr alloys are more susceptible to pitting than Ti alloys.

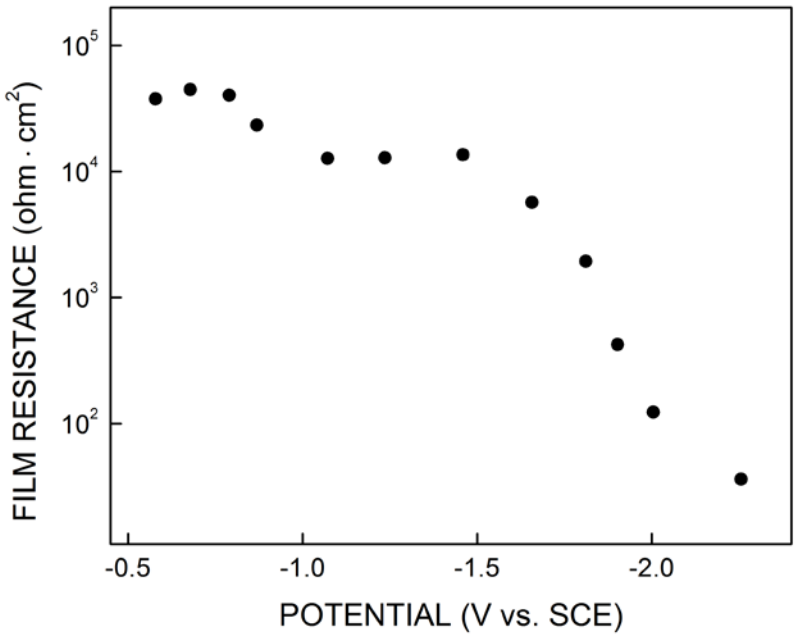

Figure 7A: Variation of the oxide film resistance on Zr-2 as a function of applied potential in a deaerated neutral 0.1 mol/L Na_2SO_4 solution. The resistance was determined by electrochemical impedance spectroscopy on an oxide pre-grown in air for 24 hours prior to exposure to the solution (Nowierski et al. 2009a, b).

Under cathodic polarization the two metals also exhibit significant differences, Figure 1A. Figures 6A and 7A (Noël et al. 2008) show the film resistances, determined by impedance spectroscopy, as the electrode is polarized to increasingly negative potentials. When comparing these two sets of behaviour, it should be noted that only the relative changes matter, not the absolute values: the latter vary due to differences in electrode pretreatment. For Ti, the film resistance begins to decrease for $E \leq -0.3$ V (vs. SCE) while that for Zr does not vary significantly until $E < -1.54$ V (vs. SCE). These values are close to the flatband potentials of −0.54 V for Ti (Torresi et al. 1987) and ~ −1.5 V (vs SCE) for Zr (Meisterjahn et al. 1987). The discrepancy in the case of Ti will be discussed below. The flatband potential is that potential at which the Fermi level in the oxide equals the redox potential in the solution and no charge (in the form of electrons) crosses the oxide/solution interface. When the potential is made more negative than the flatband value (for an n-type semiconductor) the oxide becomes degenerate and behaves like a metal allowing electron transfer to reduce H_2O to H_2 (in the present case).

For TiO_2 on Ti, once the potential is polarized negative to the flatband value, the oxide undergoes redox transformations ($Ti^{IV} \rightarrow Ti^{III}$) leading to the availability of multiple oxidation states and a consequent increase in conductivity. This facilitates electron transfer across the oxide/solution interface to reduce H_2O, a process accompanied by the absorption of H into the oxide as clearly demonstrated by neutron reflectometry (Tun et al. 1999) and illustrated schematically in Figure 8A. This coupled redox transformation-hydrogen absorption process can be described by the reaction (Ohtsuka et al. 1987)

$$TiO_2 + xH^+ + xe^- \rightarrow TiO_{2-x}(OH)_x \qquad (1A)$$

For Zr, similar redox transformations are unavailable and the very negative flatband potential means degeneracy, leading to a reduction in film resistance and the onset of H_2O reduction, is not achieved until ~ −1.5 V, Figure 7A. The absence of changes in film properties and further incorporation of H has been demonstrated by neutron reflectometry to potentials as negative as −2.5 V, Figure 9A.

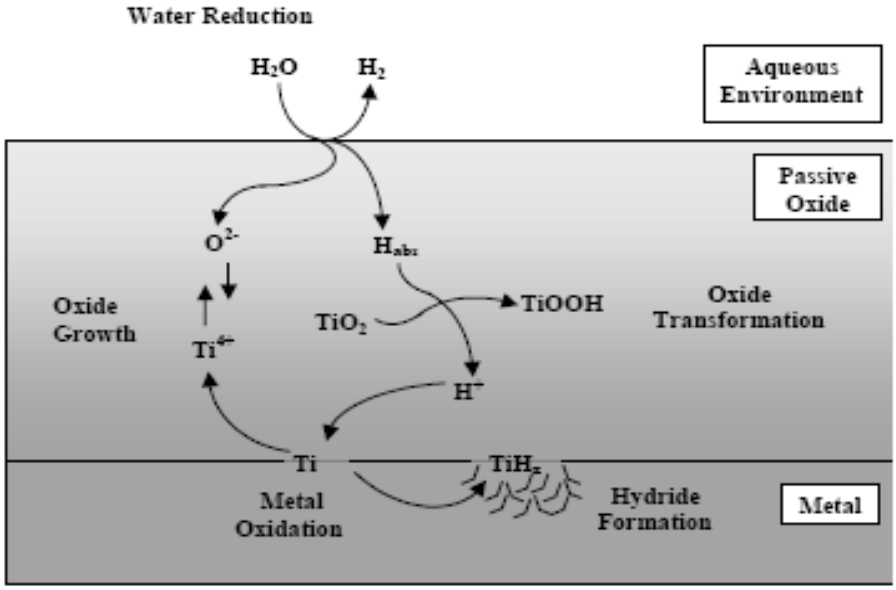

Figure 8A: Schematic illustration of the transformations in a TiO_2 film on Ti occurring under cathodic polarization leading to the absorption of H into the metal and the formation of hydrides.

Commercial Ti and Zr alloys inevitably contain small concentrations of alloying elements and impurities with limited solubility in the α-Ti or α-Zr matrix. As a consequence, they segregate to grain boundaries to form intermetallic precipitates; e.g., Fe-containing β-phase and Ti_xFe in commercially pure Ti (Grade 2; Ti-2), $Zr_2(Fe, Ni)$ and $Zr(Fe, Cr)_2$ in Zircaloys. The presence of secondary phase precipitates (SPPs) in Zircaloys does not have a major influence on the passive behaviour except at the extremes of anodic and cathodic polarization.

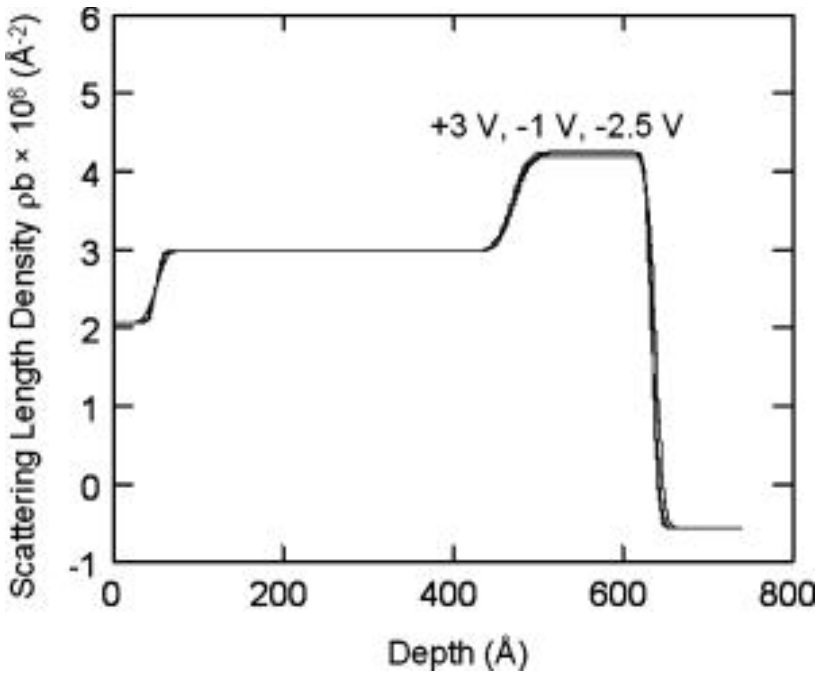

Figure 9A: Neutron reflectometry profiles recorded on Zr as a function of applied potential in a neutral 0.1 mol/L Na_2SO_4 solution. The electrode was oxidized at a series of increasingly positive potentials up to +3 V (profile shown). Subsequently, the anodically oxidized electrode was cathodically polarized to a series of more negative potentials (the profiles for −1 V and −2.5 V are shown). The similarity of the profiles shows that no significant change in the composition of the oxide occurs as a consequence of cathodic polarization (Noël et al. 2008).

This influence has recently been studied using scanning electrochemical microscopy (SECM), a technique able to probe the reactivity of individual locations on a surface with a resolution of a few microns (Zhu et al. 2007, 2008; Nowierski et al. 2009a). This is achieved by measuring the electrochemical consumption of a redox reagent, dissolved in the solution, on the alloy surface using a microelectrode, located within a few microns of the surface, to measure the current required to regenerate the consumed mediator. By scanning the microelectrode through the solution above the substrate, the reactivity of an area of the surface can be mapped.

Figure 10A shows a series of such images recorded at a single location on Ti-2 as the applied potential is made increasingly negative. A number of locations become more easily activated than the general oxide-covered surface. The black lines are drawn to interconnect these locations and their pattern is similar to that of the grain boundaries, indicating that it is the Ti_xFe precipitates at these locations which are preferentially activated. This activation occurs at potentials ~250 mV above the flatband potential, making these locations preferential sites for H_2O reduction compared to the passive oxide-covered α-matrix. Also, given the ability of these secondary phases to absorb H, they are also potential windows for H absorption into the alloy providing the corrosion potential can be polarized to these potentials under natural corrosion conditions. This process is illustrated in Figure 11A.

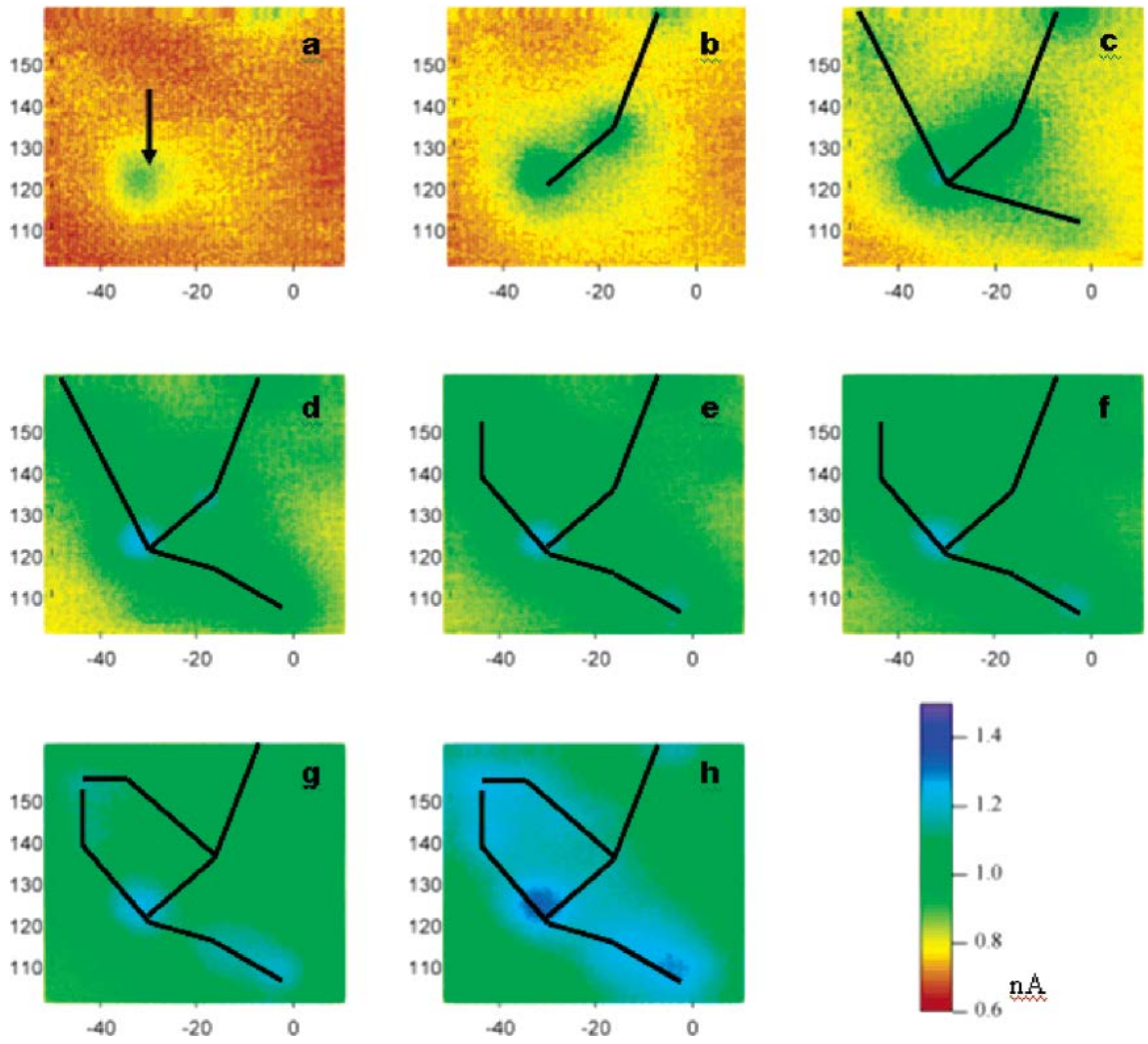

Figure 10A: Scanning electrochemical microscopy (SECM) images recorded on a single location on a Ti-2 electrode at various applied potentials in a neutral 0.1 mol/L NaCl solution. The imaged area was 60 µm x 60 µm, and all the images have the same current scale as indicated in the bottom right of the figure. The electrode was allowed to establish a steady-state corrosion potential before application of a series of increasingly negative potentials. The potentials then applied were (in V vs. SCE): (a) −0.05; (b) −0.1; (c) −0.15; (d) −0.20; (e) −0.25; (f) −0.30; (g) −0.35; and (h) −0.40 V. The initial slightly active spot is indicated by an arrow in (a). As the potential is made more negative new active locations appear. These locations are linked by black lines to indicate grain boundaries (Zhu et al. 2007).

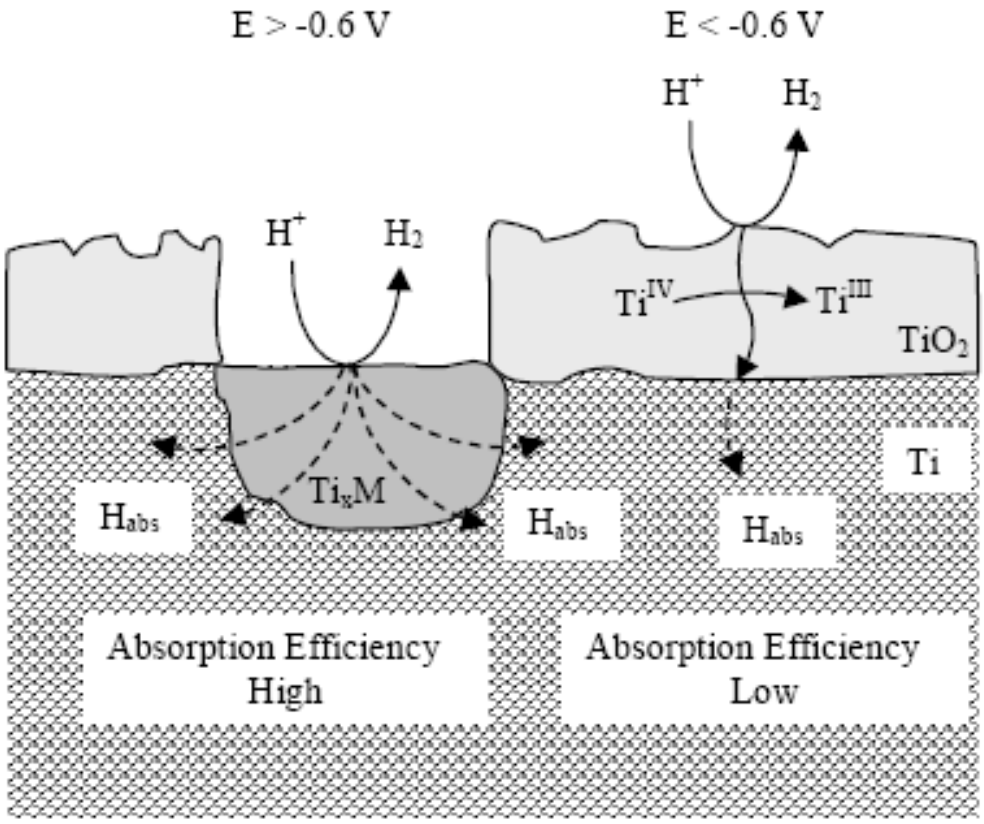

Figure 11A: Schematic illustrating the low efficiency of H absorption under passive conditions on Ti and the possibility of a higher absorption efficiency through the locations of cathodically-activated secondary phase precipitates (SPPs).

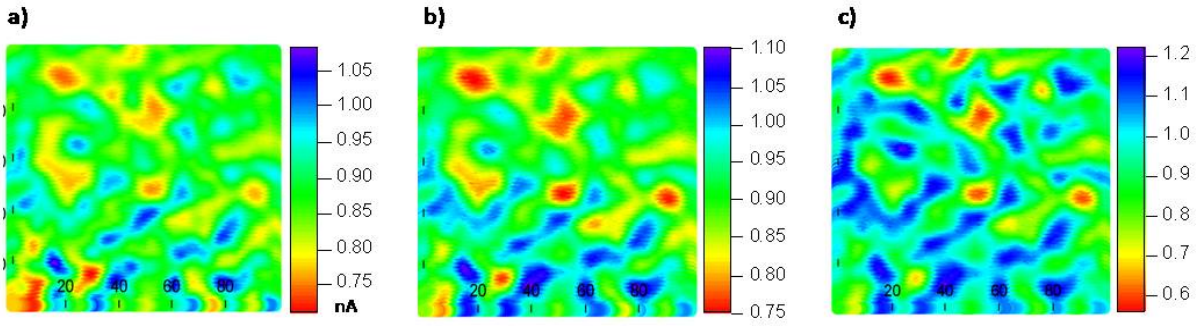

Figure 12A: Scanning electrochemical microscopy (SECM) images of the same area on an oxide-covered Zr-2 electrode at various applied potentials in a neutral 0.1 mol/L Na_2SO_4 solution. The imaged area was 100 µm x 100 µm. The electrode was allowed to establish a steady-state corrosion potential before application of a series of increasingly negative potentials. No cathodically activated locations were observed until the applied potential reached a value of −1.3 V (vs. SCE). The images show the activation of grain boundary locations at (a) −1.3 V; (b) −1.6 V; and (c) −1.9 V (vs. SCE) (Nowierski 2009).

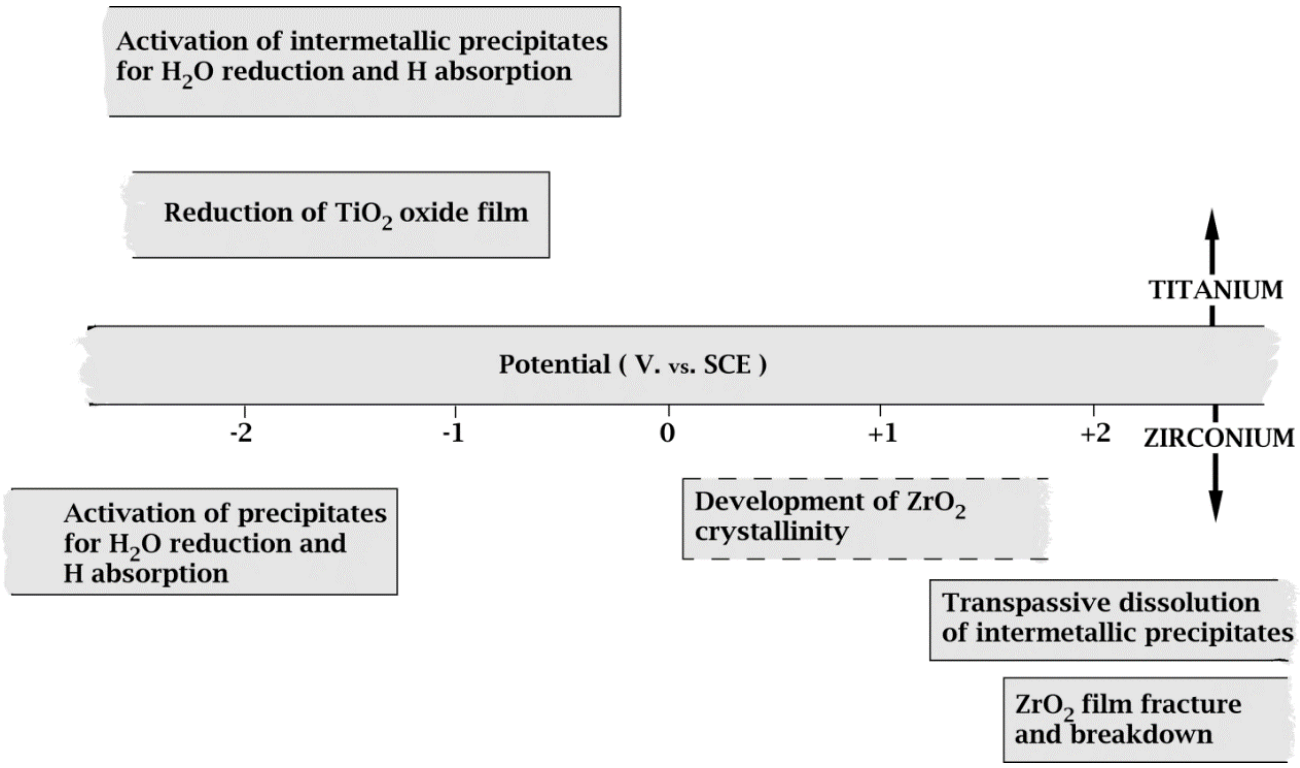

Figure 13A: Schematic showing the potential ranges within which various processes can occur on anodically or cathodically polarized Ti and Zr alloys.

Similar experiments on Zr-2 showed no indication of the activation of grain boundary precipitates and/or β-phase until the potential was ≤ –1.3 V, Figure 12A (Nowierski 2009b). These, and the neutron reflectometry results demonstrate the stability of the ZrO_2 film on Zr alloys to cathodic reduction leading to the avoidance of H absorption.

There is also published evidence to show that the presence of these SPPs does not significantly influence the anodic behaviour of either Ti or Zr alloys until the potential is polarized to values >1 V (Casillas et al. 1994, Ito and Furuya 1996). For both Ti and Zr alloys, activation of SPPs leads to the oxidation of H_2O to O_2. In the case of Ti, the presence of a thicker oxide film prevents their activation (Casillas et al. 1994) and passivity is maintained. For Zr-2 (and Zr-4) the precipitates become unstable and undergo transpassive dissolution (i.e., the conversion of Cr in the SPP particles, or Cr^{III} in the oxide covering the particles, to soluble Cr^{VI} (CrO_4^{2-})) (Ito and Furuya 1996).

An attempt to summarize these observations is shown in Figure 13A. Consistent with the polarization curves shown in Figure 1A, the passive film on Ti and its alloys is more resilient under anodic (oxidizing) conditions while that on Zr and its alloys is more resilient under cathodic (reducing) conditions.

REFERENCES.

Been, J. and J.S. Grauman. 2000. Titanium and titanium alloys In: Uhlig's Corrosion Handbook, 2nd Edition, Revie, R.W. editor. Chapter 47. John Wiley: New York, New York.

Casillas, N., S. Charlebois, W.H. Smyrl and H.S. White. 1994. Pitting corrosion of titanium. Journal of Electrochemical Society, 141, 636-642.

Cox, B. 1970. Factors affecting the growth of porous anodic oxide films on zirconium. Journal of Electrochemical Society, 117, 654-663.

Ito, Y. and T. Furuya. 1996. Correlation between electrochemical properties and corrosion resistance of zirconium alloys. In: Zirconium in the Nuclear Industry: Eleventh International Symposium, ASTM STP 1295, E.R. Bradley and G.P. Sabol, Eds. American Society for Testing and Materials, 163-180.

Jarzebski, Z.M. 1973. Oxide semiconductors International Series of Monographs in Science of the Solid-State, Volume 4. Pergamon Press: New York, New York.

Jensen, H. 2002. Properties of anodic oxide films on zirconium alloys. Ph.D. Thesis, The University of Western Ontario, London, Ontario, Canada.

Khalil, N. and J.S.L. Leach. 1986. The anodic oxidation of valve metals – Determination of ionic transport numbers by α-spectrometry. Electrochimica Acta, 31, 1279-1285.

Leach, J.S.L. and B.R. Pearson. 1988. Crystallization in anodic oxide films. Corrosion Science, 28, 43-56.

Meisterjahn, P., H.W. Hoppe and J.W. Schultze. 1987. Electrochemical and XPS measurements on thin oxide films on zirconium. Journal of Electroanalytical Chemistry, 217, 159-185.

Noël, J.J. H.L. Jensen, Z. Tun and D.W. Shoesmith. 2000. Electrochemical modification of the passive oxide layer on Zr-2.5Nb observed by in-situ neutron reflectometry and scanning electron microscopy. Electrochemistry Communications, 11, 1234-1236.

Noël, J.J., D.W. Shoesmith and Z. Tun. 2008. Anodic oxide growth and hydrogen absorption on Zr in neutral aqueous solution. A comparison to Ti. Journal of Electrochemical Society, 155, C444-C454.

Nowierski, C., J.J. Noël, D.W. Shoesmith and Z. Ding. 2009a. Correlating surface microstructures with reactivity on commercially pure zirconium using scanning electrochemical microscopy and scanning electron microscopy. Electrochemistry Communications, 11, 1234-1236.

Nowierski, C. 2009b. Analysis of the electrochemistry and surface microstructure of zirconium alloys under cathodic polarization. M.Sc. Thesis, The University of Western Ontario, London, Ontario, Canada.

Ortega, C. and J. Siejka. 1982. A study by nuclear microanalysis and ^{18}O tracing of the growth of anodic oxide films on zirconium. Journal of Electrochemical Society, 129, 1905-1917.

Ohtsuka, T., M. Masuda and N. Sato. 1987. Cathodic reduction of anodic oxide films formed on titanium. Journal of Electrochemical Society, 134, 2406-2410.

Schutz, R.W. and D.E. Thomas. 1987. Corrosion of Titanium and Titanium alloys. In: Corrosion 13, 669-706. ASM Metals Handbook.

Shibata, T. and Y.-C. Zhu. 1995. The effect of film formation conditions on the structure and composition of anodic oxide films on titanium. Corrosion Science, 37, 253-270.

Shoesmith, D.W. and B.M. Ikeda. 1997. The resistance of titanium to pitting, microbially induced corrosion and corrosion under unsaturated conditions. Atomic Energy of Canada Limited Report AECL-11709, COG-96-557-1. Chalk River, Canada.

Shoesmith, D.W. and J.J. Noël. 2010. Corrosion of titanium and its alloys, In: Shreir's Corrosion, Richardson, J.A. et al. editors, Volume 3, 2042-2052. Elsevier, Amsterdam.

Torresi, R.M., O.R. Cámara, C.P. DePauli and M.C. Giordano. 1987. Hydrogen evolution reactions on anodic titanium oxide films. Electrochimica Acta 32, 1291-1301.

Tun, Z., J.J. Noël and D.W. Shoesmith. 1999. Electrochemical modification of the passive oxide layer on a Ti film observed by in-situ neutron reflectometry. Journal of Electrochemical Society, 146, 988-994.

Zeng, Y. 2009. Passive film properties and their influence on hydrogen absorption into titanium. Ph.D. Thesis, University of Western Ontario, London, Canada.

Zhu, R., C. Nowierski, Z. Ding, J.J. Noël and D.W. Shoesmith. 2007. Insights into grain structures and their reactivity on Grade-2 Ti alloy surfaces by scanning electrochemical microscopy. Chemistry of Materials, 19, 2533-2543.

Zhu, R., Z. Qin, D.W. Shoesmith and Z. Ding. 2008. Analyzing the influence of alloying elements and impurities on the localized reactivity of titanium Grade-7 by scanning electrochemical microscopy. Analytical Chemistry, 80, 1437-1447.

APPENDIX B.

B.1 PASSIVE CORROSION OF TITANIUM ALLOYS UNDER WASTE DISPOSAL CONDITIONS

The passive corrosion of titanium and its alloys has been studied in the USDOE Yucca Mountain project and other national waste disposal programs. In the Yucca Mountain project, the passive corrosion of Ti Grade-16 (Ti with a Pd content of 0.04 to 0.08 wt%) was studied in a number of aggressive simulated groundwaters (60°C and 90°C over the pH range 2.7 to 12) using weight loss measurements (Hua et al. 2004, 2005). The [Cl^-] in the solutions ranged from 67 mg/L to 178,000 mg/L which are comparable to those anticipated in crystalline and sedimentary rock environments (Table 2). No discernible dependence of the corrosion rate on temperature, pH or salinity was observed. As expected, (section 8) the corrosion rates decreased with time as the oxide on the freshly prepared specimens thickened and became less defective. Over a 5-year period, the rates decreased from >100 nm/a to between 20 and 0 nm/a, as shown by the distribution of (penetration) rates for many specimens in Figure 1B.

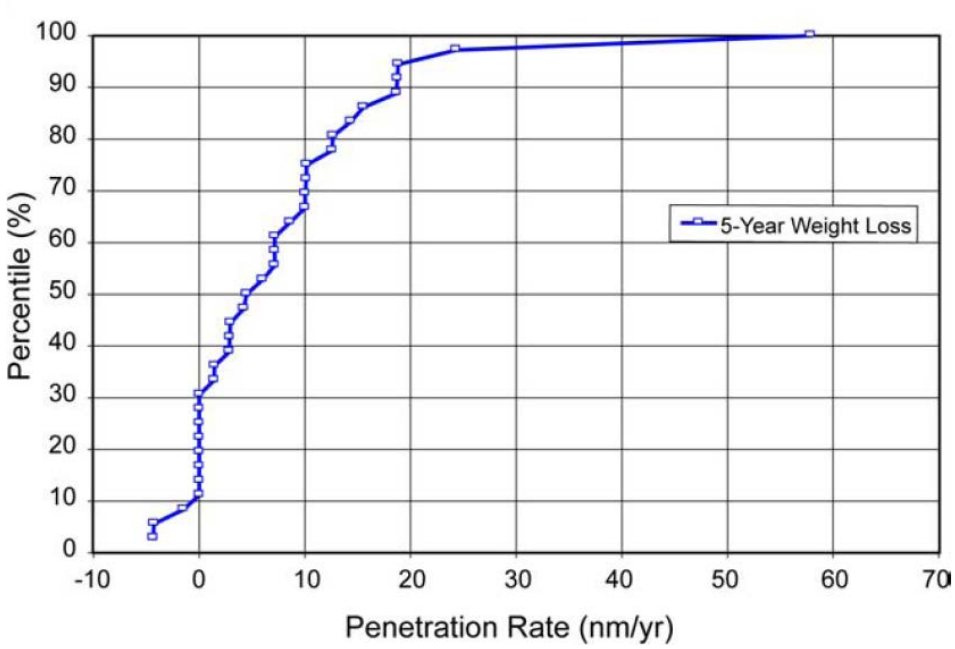

Figure 1B: Distribution of the passive corrosion rates of the Pd-containing Ti alloy, Grade-16, measured after exposure to a number of concentrated saline groundwaters (Hua et al. 2005 a, b, c).

The two values >20 nm/a and the apparently negative corrosion rates shown in the figure reflect the uncertainties in making measurements by weight change and a need to remove salts deposited from the simulated groundwaters.

These low values are consistent with a wealth of other measurements made using a range of different techniques. Mattson and Olefjord (1990), using a combination of depth profiling by ion

sputtering and X-ray photoelectron spectroscopy (XPS), measured (over a 6 year period) rates in the range 0.5 to 4 nm/a on Ti-2 and Ti-7 in compacted clays saturated with saline solutions at 95°C. Kim and Oriani [1987a, 1987b] measured (over a 2 year exposure period) rates of 40–60 nm/year in $MgCl_2$-dominated brine using ion sputtering and Auger spectroscopy, and found only a marginal increase in rate between 25°C and 108°C (the boiling point of the brine). A similar absence of any temperature dependence (90°C to 200°C) was observed by Smailos et al. (1986, 1987) for Ti-7 in very aggressive German Q-brines (NaCl 4.7%; $MgCl_2$; $MgSO_4$ 1.4%; H_2O 65.7%; pH = 4.9 at 25 °C) over an exposure period of 3.5 years. Even at 250°C, Molecke et al (1982) found a corrosion rate for Ti-7 of only 400 nm/a in aerated brine.

REFERENCES

Hua, F., K. Mon, P. Pasupathi, G.M. Gordon and D.W. Shoesmith. 2004. Corrosion of Grade-7 and other Ti alloys in nuclear waste repository environments – A review. Corrosion 2004, Paper No. 04689, National Association of Corrosion Engineers, Houston, Texas, USA.

Hua, F., K. Mon, P.Pasupathi, G.M. Gordon and D.W. Shoesmith. 2005. A review of corrosion of titanium Grade-7 and other titanium alloys in nuclear waste repository environments. Corrosion, 61, 987-1003.

Kim, Y.J. and R.A. Oriani. 1987a. Brine radiolysis and its effect on the corrosion of Grade-12 titanium. Corrosion, 43, 92-97.

Kim, Y.J. and R.A. Oriani. 1987b. Corrosion properties of the oxide film formed on Grade-12 titanium in brine under gamma radiation. Corrosion, 43, 85-91.

Mattsson, H. and I. Olefjord. 1990. Analysis of oxide formed on Ti during exposure in bentonite clay – 1, The oxide growth. Werkstoffe und Korrosion, 41, 383-390.

Molecke, M.A., J.A. Ruppen and R.B. Diegle. 1982. Materials for high-level canister/overpacks in salt formations. Sandia National Laboratory Report SAND 82-0429.

Smailos, E., W.SCHwarzkopf and R. Koster. 1986. Corrosion behaviour of container materials for disposal of high-level wastes in rock salt environments, Nuclear Science and Engineering, Commission of the European Communities, Luxembourg, EUR-10400-EN.

Smailos, E. and R. Koster. 1987. Corrosion studies on selected packaging materials for disposal of high-level wastes. In: Materials Reliability in the Back End of the Nuclear Fuel Cycle. International Atomic Energy Agency TECDOC-421, 7-24, IAEA, Vienna, Austria.